CHAPTER

3

THE INFLUENCE OF PRESSURE ON THE PROPERTIES AND ORIGINS OF HYDROUS SILICATE LIQUIDS IN EARTH'S INTERIOR

Craig E. Manning
University of California, Los Angeles, CA, United States

CHAPTER OUTLINE

1. INTRODUCTION

Earth is distinct from other terrestrial planets in part because of its endowment with more H_2O. Water influences a wide range of terrestrial processes, but few so dramatically as terrestrial silicate magmatism. Water participates in the generation of silicate magmas when it is present in rock-forming minerals, and/or in pore fluids, yielding a greater range of liquid compositions and stability than would obtain in a dry planet.

Water plays a significant role in the production of silicate liquids from the surface to at least as deep as the base of the mantle transition zone. Minor H_2O in mantle minerals expands the melting regime

Magmas Under Pressure. https://doi.org/10.1016/B978-0-12-811301-1.00003-4

during generation of midocean ridge basalts (Hirth and Kohlsetdt, 1996; Asimow and Langmuir, 2003; Asimow et al., 2004) and ocean island basalts (Aubaud et al., 2004; Hirschmann, 2006). Subduction carries H_2O into the mantle, bound as hydroxyl (or less commonly as molecular H_2O) in hydrous minerals and as a trace constituent in nominally anhydrous minerals. Redistribution of H_2O during slab metamorphism can trigger melting, dehydration, and/or diapiric rise of buoyant hydrous slab material (Poli and Schmidt, 1995, 2002; Schmidt and Poli, 1998; Gerya and Yuen, 2003; van Keken et al., 2011). The upward transfer of H_2O-bearing materials contributes to mantle melting at convergent margins (Kushiro, 1990; Ulmer, 2001; Grove et al., 2006; Till et al., 2012), producing basaltic liquids richer in H_2O than those in other settings (e.g., Grove et al., 2012; Plank et al., 2013). Some hydrous mantle melts are transported to the surface to erupt, while others are trapped in the crust where they transfer their heat and H_2O (and other volatiles) to generate crustal melts. The interplay of melting, H_2O transfer, and melt migration is expressed in the complex, crustal-scale plumbing systems of magmatic arcs (Annen et al., 2006; Cashman et al., 2017), and ultimately facilitates the magma-assisted generation of continental crust (e.g., Campbell and Taylor, 1983) and powers the explosive eruptions characteristic of this tectonic setting.

The H_2O retained in the subducting lithosphere is carried farther into the mantle, where it may contribute to back-arc basalt genesis (e.g., Stolper and Newman, 1994; Kelley et al., 2006, 2010) and very likely to melt generation in deeper mantle environments. Slab stagnation in or passage through the mantle transition zone, coupled with comparatively high H_2O in wadsleyite and ringwoodite (Kohlstedt et al., 1996; Bolfan-Casanova, 2005), may contribute to elevated water concentrations in this part of the mantle (Pearson et al., 2014; Palot et al., 2016), with important consequences for deep generation of hydrous silicate melts (Bercovici and Karato, 2003; Karato et al., 2006; Karato, 2011). Geophysical studies identify possible melt at and above the 410-km discontinuity (e.g., Revenaugh and Sipkin, 1994; Toffelmier and Tyburczy, 2007; Tauzin et al., 2010), which could be neutrally buoyant and therefore gravitationally stable for significant time (Matsukage et al., 2005; Sakamaki et al., 2006). Similar regions have been inferred just below 660 km (Schmandt et al., 2014; Liu et al., 2016). Water-bearing melts derived from local upwelling of hydrous transition-zone rocks could produce voluminous continental flood basalts (Wang et al., 2015). Finally, the oceanic low-velocity zone may be caused, at least locally, by a spatially discontinuous layer of melt stabilized by the presence of H_2O in the liquid (Hirschmann, 2010, and references therein; Schmerr, 2012; Sakamaki et al., 2013; Beghein et al., 2014). A similar layer of hydrous melt may occur at the lithosphere−asthenosphere boundary beneath continents (Crépisson et al., 2014).

In each case above, melt genesis and transport at elevated pressure are strongly influenced by H_2O. The addition of even minor H_2O to an anhydrous silicate-dominated rock causes a strong decrease in the melting temperature at a given pressure. The effect is common to all silicate systems and it is amplified by compression. This makes it possible for silicate systems to melt at lower temperature than they otherwise might, regardless of their composition. The solubility of H_2O in silicate magmas is low at ambient pressure but rises dramatically as pressure increases. Thus, silicate melts are important transport agents for H_2O and they play a central role in the planetary water cycle (Hirschmann, 2006; Hirschmann and Kohlstedt, 2012). H_2O strongly modifies primary melt compositions and liquid lines of descent, so it helps modulate planetary differentiation processes. The addition of H_2O also fundamentally changes melt physical properties, strongly influencing rates and direction of movement, connectivity, viscosity, diffusivity, electrical conductivity, and seismic velocities.

The role of H_2O in silicate melts has been widely studied and reviewed (e.g., Burnham, 1979, 1997; Mysen, 1988; Johannes and Holtz, 1996; Mysen and Richet, 2005). Here I focus on the influence of pressure on the generation and properties of hydrous silicate melts. I start with the dramatic increase in H_2O solubility with pressure. I then review solution mechanisms and melt structure, illustrating that the manner in which H_2O interacts with silicate components in the liquid exerts a primary control on phase equilibria and mixing properties of H_2O and silicate melts. After establishing the links between H_2O solubility, solubility mechanisms, and the generation of hydrous silicate melts, I turn to the role of pressure on the physical properties of hydrous melts. A common theme is that advances in experimental techniques coupled with the growing capabilities of first-principles computational methods are overcoming the limitations of studies based on quenched liquids, leading to improved understanding of hydrous silicate melts at depth in the crust and mantle.

2. H_2O SOLUBILITY AND SPECIATION IN SILICATE LIQUIDS

2.1 H_2O SOLUBILITY

A convenient starting point for understanding the role of H_2O is through the changes in its solubility in silicate melts with pressure up to ~0.5 GPa (e.g., Dingwell, 1986) (relations at higher pressure are considered later). Experimental data on the solubility of H_2O in $NaAlSi_3O_8$ melts (Fig. 3.1A) indicate

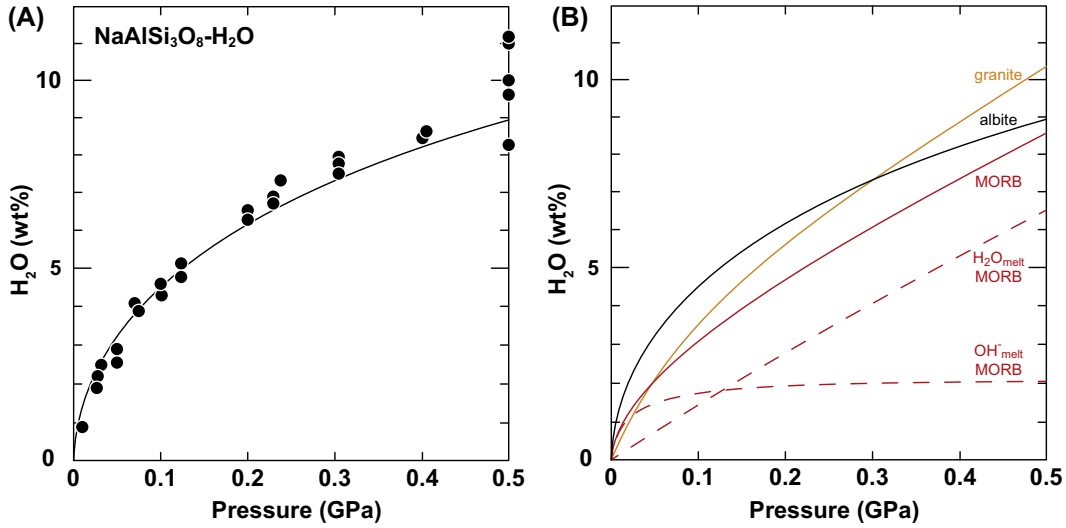

FIGURE 3.1

(A) Variation in H_2O solubility in $NaAlSi_3O_8$ melt with pressure. *Filled circles*, experimentally determined H_2O solubility at 1098−1400°C, compiled by Silver and Stolper (1989). *Solid line*, calculated solubility at 1200°C, assuming ideal mixing of OH^-_{melt}, H_2O_{melt}, O^{2-}_{melt} (Stolper, 1982a,b; Silver and Stolper, 1989). (B) Variation in H_2O solubility with pressure in albite liquid (1200°C), midocean ridge basalt (MORB, 1200°C, Dixon et al., 1995), and haplogranite (1000°C, Holtz et al., 1995). *Dashed lines* show speciation of OH^-_{melt}, H_2O_{melt} in MORB (Dixon et al., 1995).

that H_2O concentration at vapor saturation rises with pressure. At ambient pressure, H_2O is effectively insoluble in the liquid, but as pressure increases to about 0.5 GPa, the concentration rises to 9–10 wt%, or ~60 mol%. Thus, with a relatively modest change in pressure, the ability of the silicate liquid to dissolve H_2O increases to the point that, on a molar basis, it contains more H_2O than $NaAlSi_3O_8$.

The solubility behavior exhibited by H_2O in $NaAlSi_3O_8$ liquid is also seen in more complex compositions, including simple granite and basalt (Fig. 3.1B), as well as other natural liquids with a range of alkalinity and silica content (e.g., Moore et al., 1998). The H_2O solubility pattern in each composition is similar: it initially increases steeply with compression at near ambient pressure, but the increase shallows once pressures rise above about 0.2 GPa.

2.2 SOLUBILITY MECHANISMS

At the pressures shown in Fig. 3.1, H_2O dissolves into silicate melts by forming two main species, molecular H_2O (H_2O_{melt}) and hydroxyl $\left(OH^-_{melt}\right)$ (Stolper, 1982a, and references therein). The relative abundance of the two species changes with pressure, temperature, and composition, modulated by interaction with oxygen in the silicate melt $\left(O^{2-}_{melt}\right)$. Homogeneous equilibrium at a given pressure and temperature and composition can thus be described by

$$H_2O_{melt} + O^{2-}_{melt} = 2OH^-_{melt}, \tag{3.1}$$

for which

$$K_1 = \frac{a^2_{OH^-_{melt}}}{a_{H_2O_{melt}} a_{O^{2-}_{melt}}}, \tag{3.2}$$

where K is the equilibrium constant and a is activity of the subscripted species. At relatively low H_2O concentrations, mixing is nearly ideal and activity coefficients are unity (Stolper, 1982a; Silver and Stolper, 1985, 1989; Silver et al., 1990). Activities can therefore be replaced by mole fractions in Eq. (3.2) (1 oxygen basis), and knowledge of K_1 values can be used to investigate species distribution in hydrous liquids. Early experimental determinations of K_1 were based on quenched hydrous glasses, which require rapid quenching (e.g., Zhang, 1999 and references therein). However, as reviewed by Zhang (1999), even with rapid quenching it is difficult to obtain accurate species distribution for magmatic T due to the rapid rates of Reaction (3.1) and the T dependence of IR extinction coefficients. While quenched glasses can furnish useful quantitative information, at least at low magmatic T, alternative approaches are desirable. The development of diamond cell methods for in situ infrared (IR) spectroscopy at high pressure and high temperature greatly clarified results based on quenched glasses and allowed investigation to higher H_2O contents (Shen and Keppler, 1995; Sowerby and Keppler, 1999). However, in situ techniques also come with tradeoffs: they require careful calibration, have lower precision, and bulk H_2O concentration is difficult to constrain.

An alternative, indirect approach is to exploit experimentally determined variations in liquidus surfaces with H_2O concentrations. Fig. 3.2 gives examples using recent results on the system $NaAlSi_3O_8$–H_2O at 1 GPa (Makhluf et al., 2016). Assuming ideal mixing (Stolper, 1982a; Silver and Stolper, 1989) yields $K_1 = 0.254$ at 1000°C. As shown in Fig. 3.2A, OH^-_{melt} is the dominant species at all H_2O concentrations to the liquidus value of 4.2 wt%. In contrast, near H_2O-saturated melting at 700°C, K_1 is lower (0.014), liquidus H_2O content is much higher, and H_2O_{melt} predominates over nearly the entire range of H_2O concentration (Fig. 3.2B). The value of K_1 decreases with temperature

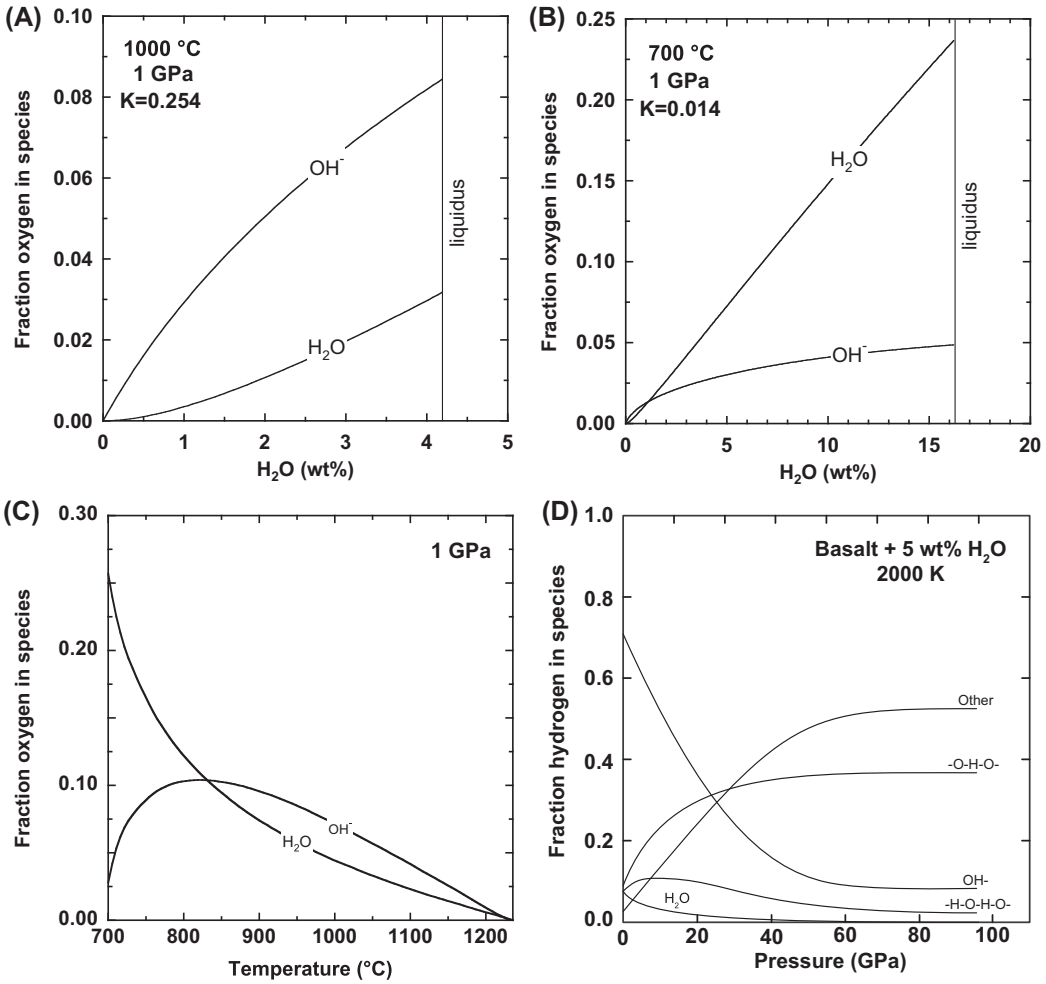

FIGURE 3.2

(A)–(C) Speciation of OH^-_{melt}, H_2O_{melt} in hydrous $NaAlSi_3O_8$ melt at 1 GPa based on the results of Makhluf et al. (2016). Calculations used thermodynamic data for albite and albite liquid from Holland and Powell (1998, 2002 update) and assumed ideal mixing. Panel (C) shows speciation along the liquidus; H_2O concentration increases with decreasing temperature. (D) Change in the abundance of H species with pressure in basalt with 5 wt% H_2O (30 mol% H) at 2000K. Results based on first principles simulations of Bajgain et al. (2015).

(Silver and Stolper, 1989; Zhang, 1999), leading to a change in speciation along the liquidus (Fig. 3.2C). Thus, at the liquidus, OH^-_{melt} generally predominates at higher temperature where bulk H_2O is lower, whereas molecular H_2O predominates at lower temperature and higher bulk H_2O concentrations. Note that if the restriction of equilibrium with crystals is removed (i.e., at supra-liquidus conditions), H_2O_{melt} will increase with bulk H_2O concentration.

The general trends for the speciation of water in natural silicate melts are broadly similar to those in $NaAlSi_3O_8$ melts at crustal and uppermost mantle pressures. For example, Fig. 3.1B illustrates the variation in the abundance of OH^-_{melt} and H_2O_{melt} with pressure at 1200°C in midocean ridge basalt (MORB). As pressure increases, H_2O_{melt} becomes the predominant species at ~0.2 GPa.

A key conclusion for relatively low pressures of the lower crust and upper mantle is that OH^-_{melt} is the predominant species at low bulk H_2O concentrations and high temperatures. At high bulk H_2O concentrations and relatively low temperature, H_2O_{melt} is the predominant species. However, additional species likely become relevant at higher pressures. For example, at 6 and 13 GPa in the $MgO-SiO_2-H_2O$ system, liquidi can generally be explained by the temperature variation of K_1, but the model fails to fit liquidi for SiO_2-H_2O and $MgSiO_3-H_2O$ at 13 GPa (Myhill et al., 2017; Novella et al., 2017).

Ab initio molecular dynamics studies provide insights into this problem. Work on SiO_2-H_2O indicates that at a pressure of ~4 GPa, hydroxyl and molecular H_2O predominate (Pöhlmann et al., 2004; Anderson et al., 2008; Spiekermann et al., 2016). At the very high temperature of these simulations (≥2400 K), OH^- greatly exceeds molecular H_2O in abundance, consistent with increasing K_1 with temperature. Mookherjee et al. (2008) carried out first principles molecular dynamics simulations on $MgSiO_3-H_2O$ to conditions approaching the base of the mantle (~135 GPa). They found that at pressures higher than those of the upper mantle, OH^- and molecular H_2O species give way to extended structures involving Si−O−H−O−Si and Si−O−H−O−H−O−Si interpolyhedral bridges. Similar results are found for more polymerized SiO_2 melts (Karki and Stixrude, 2010) and basalt−H_2O (Bajgain et al., 2015). These additional forms of H_2O incorporation could explain why high-pressure liquidus relations in the $MgO-SiO_2-H_2O$ system cannot be fit by simple speciation of OH^- and molecular H_2O (Myhill et al., 2017; Novella et al., 2017). However, it is not yet possible to derive equilibrium constants for homogeneous equilibria involving these species.

2.3 EFFECTS ON MELT STRUCTURE

Silicate melts can be modeled as variably polymerized oxide liquids composed of network-forming cations (chiefly Si^{+4} and Al^{+3}) and network-modifying metal cations (Toop and Samis, 1962; Hess, 1971, 1980; Mysen and Richet, 2005, and references therein). Polymerized aluminosilicate melts are dominated by O^{2-}_{melt} in bridging, network-forming positions. In anhydrous liquids, compression leads to a decrease in nonbridging oxygens in favor of higher O coordination numbers about network-forming Si and Al (e.g., Lee et al., 2004). Similar trends are seen in anhydrous and hydrous liquids, but at a given pressure and temperature, H_2O decreases O−Si and O−Al coordination (Mookherjee et al., 2008; Bajgain et al., 2015). For a given pressure, temperature, and coordination environment, addition of H_2O shifts Eq. (3.1) to the right, replacing bridging O^{2-}_{melt} with two OH^-. Thus, H_2O acts as a network modifier in silicate liquids, regardless of pressure.

The role of H_2O on silicate melt polymerization has been widely studied. An extensive literature on quenched glasses (e.g., see Mysen and Richet, 2005) yields fundamental insights but is problematic due to large changes in glass structure with temperature (and pressure). However, as with speciation, in situ experimental approaches and first-principles computational methods are now adding significantly to our understanding of hydrous melt structure at high pressure.

Fig. 3.3A provides an example confirming that addition of H_2O depolymerizes silicate liquids. Using the concentration of nonbridging O^{2-}_{melt} (NBO) relative to tetrahedral cations (T) as a measure of

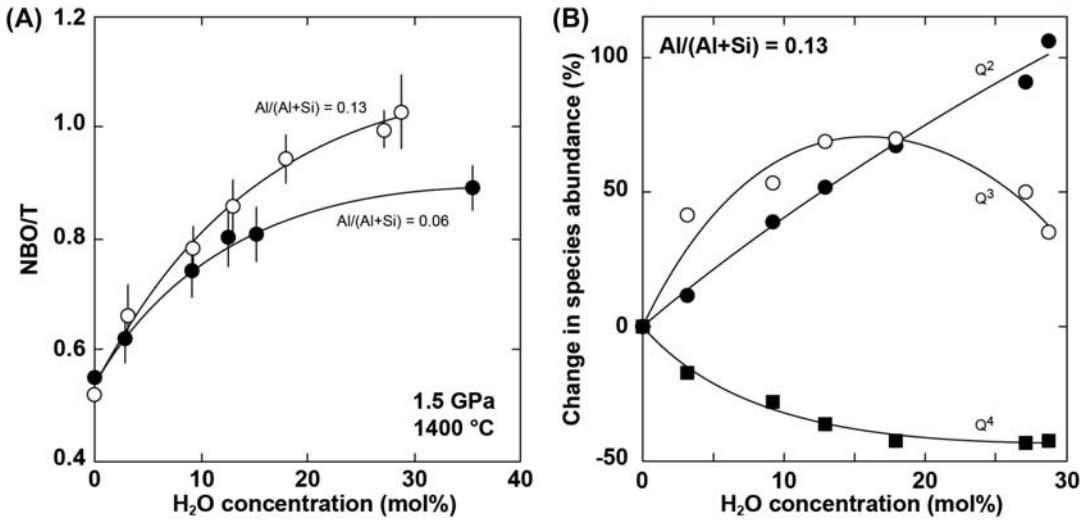

FIGURE 3.3

(A) Variation in NBO/T with H_2O concentration in sodium aluminosilicate melts at 1400°C and 1.5 GPa (Mysen, 2007, 2014). (B) Change in abundance of Q^n species as a function of H_2O concentration in Na aluminosilicate glasses quenched from 1400°C, 1.5 GPa (Mysen, 2007, 2014).

the extent of polymerization (polymerization decreases with rising NBO/T), Mysen (2007) showed that increasing H_2O concentration correlates with increasing NBO/T in alkali aluminosilicate melts at 1.5 GPa and 1400°C. Regardless of bulk composition, addition of H_2O yields a greater degree of depolymerization at low H_2O relative to high H_2O. This is consistent with the expectation that OH^-_{melt} is most abundant at low bulk H_2O concentration, whereas H_2O_{melt} predominates at higher bulk H_2O (Fig. 3.2). Evidently both species disrupt the network, but OH^-_{melt} does so to a greater degree. Fig. 3.3B shows the effect on the abundance of specific oligomers in the melt (Q^4, TO_2; Q^3, $TO_{2.5}$, …, Q^0, TO_4, where T is a tetrahedrally coordinated cation). The most polymerized species (Q^4) decrease in abundance with rising H_2O, whereas less polymerized Q^2 species increase. Note that Q^3 species increase to a maximum at ~15 mol% H_2O and then decline.

3. EFFECT OF PRESSURE ON HYDROUS MELTING

3.1 HYDROUS MELTING AT LOW TO MODERATE PRESSURE

At elevated pressure, the addition of H_2O decreases the temperature of melting of silicate rocks. Fig. 3.4A illustrates the effect of H_2O on melting of diopside:

$$\underset{\text{diopside}}{CaMgSi_2O_6} = \underset{\text{melt}}{CaMgSi_2O_6} \tag{3.3}$$

The preferred dissolution of H_2O into the melt relative to diopside reduces the activity of $CaMgSi_2O_6$ melt (Eq. 3.3), isobarically shifting the melting point to a lower temperature. The more the H_2O

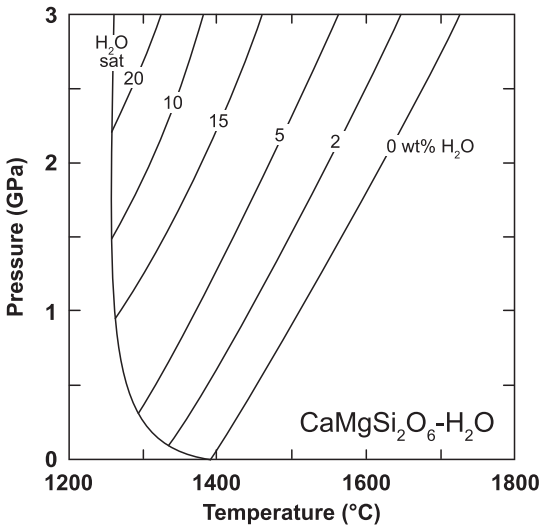

FIGURE 3.4

Melting phase relations for the system $CaMgSi_2O_6$–H_2O (after Perchuk and Kushiro, 1991).

dissolved, the greater the decrease in melting temperature. The polythermal, polybaric loci of melting points for a given H_2O content define the H_2O solubility isopleths (Fig. 3.4). Where the maximum capacity to dissolve H_2O is reached, melting occurs in the presence of a saturated H_2O-rich fluid phase.

A vast number of high-pressure experimental investigations have been carried out to explore melting temperatures, liquidi, H_2O solubility, and H_2O-saturated melting conditions. A detailed review is beyond the scope of this chapter. However, three points are important in considering the properties of hydrous silicate melts at high pressure.

First, it is extremely challenging to constrain experimentally the polybaric liquidus surfaces at H_2O undersaturation. High-pressure solubility relations such as those shown in Fig. 3.4 are poorly known even for simple systems. Isopleths of H_2O concentration are typically derived from experiments and/or thermodynamic modeling, and link liquidus phase relations with H_2O speciation and activity. High-pressure examples include $NaAlSi_3O_8$–H_2O (Makhluf et al., 2016), $CaMgSi_2O_6$–H_2O (Perchuk and Kushiro, 1991), and MgO–SiO_2–H_2O (Inoue, 1994; Myhill et al., 2017; Novella et al., 2017). Such systematic studies are nearly impossible for complex natural systems. Examples of the challenges can be seen in a recent study of the haplogranite liquidus (Makhluf et al., 2017a), which required well over 100 individual experiments, some of over 1 week in duration. An alternative is melting models based on experimental results covering a range of pressure, temperature, and composition (e.g., Katz et al., 2003, and references therein). Regardless, simple but important generalizations are that (1) H_2O always lowers the melting point of any silicate system and (2) H_2O solubility isopleths have a positive dependence on pressure, so H_2O solubility in silicate melt always increases with rising pressure at constant temperature (e.g., Fig. 3.4).

A second point involves H_2O-saturated melting of natural compositions, which is essential for establishing minimum melting temperatures as a function of pressure. There still remain fairly large

discrepancies for systems important for high-pressure environments, most importantly here, peridotite−H_2O. Early work on H_2O-saturated peridotite melting gave conflicting results. Kushiro et al. (1968a) showed that in the presence of H_2O, the maximum depression of the anhydrous solidus for spinel peridotite is to about 1000°C at 3 GPa. Several subsequent studies yielded similar results (Green, 1973; Millhollen et al., 1974; Kawamoto and Holloway, 1997). However, Mysen and Boettcher (1975) found much lower melting temperature of ~800°C at the same conditions. Grove et al. (2006) revisited the problem and identified evidence for H_2O-saturated melting at temperatures similar to Mysen and Boettcher. Key to the results is the interpretation of quench products. Green et al. (2010) suggested that the material identified by Grove et al. (2006) as quenched melt was actually precipitate from a subsolidus, solute-rich fluid phase. Till et al. (2012) and Grove et al. (2012) reconfirmed the results of Grove et al. (2006), noting problems with Green et al.'s quench interpretations, compositional criteria, and run durations. Thus, it remains possible, if not likely, that hydrous peridotite melting may occur at surprisingly low temperatures.

Finally, H_2O plays a crucial role in melt composition and melt fraction, with important consequences for the properties of hydrous silicate melts. Early work on MgO−SiO_2−H_2O established that in the presence of H_2O, incongruent melting of enstatite persists to high pressure, yielding SiO_2-oversaturated liquids (Kushiro et al., 1968b). This led to the proposal that hydrous mantle melting produced primary andesitic magmas, potentially explaining their common occurrence at convergent margins. However, SiO_2-undersaturated basalts are also abundant in this setting, and later studies showed that hydrous peridotite melting typically produces hydrous basaltic liquids (e.g., Green, 1973; Gaetani and Grove, 1998). H_2O increases melt fractions, changes the compositions of primary hydrous basaltic melts, and modifies liquidus phases (Gaetani and Grove, 1998; Müntener et al., 2001). H_2O also changes the liquid line of descent, as in basalts where H_2O differences can lead to a calc−alkaline versus tholeiitic trend. Similar effects are seen in other compositional systems. For example, high-pressure hydrous melting of garnet peridotite yields liquids poorer in MgO and CaO and richer in SiO_2 and A_2O_3 than in the absence of water (Tenner et al., 2012); trace element partitioning is also strongly affected (Kessel et al., 2015). At the other end of the compositional spectrum, high-pressure melting of subducted sediments produces compositions that may be trondhjemite, metaluminous granite, or peraluminous granite, depending on pressure and temperature (Schmidt et al., 2004; Hermann and Spandler, 2008; Mann and Schmidt, 2015), which can lead to important variations in physical properties (Schmidt, 2015). In short, consideration of the properties of hydrous silicate melts at high pressure demands the recognition that H_2O also intermediates the composition, evolution, and abundance of liquid produced.

3.2 HYDROUS MELTING AT HIGH PRESSURE: SUPERCRITICAL FLUIDS

The increase in the solubility of H_2O along the H_2O-saturated solidus in albite and diopside is portrayed over a limited range of pressure (Figs. 3.1 and 3.4). At higher pressures, H_2O solubilities in all silicate systems grow at an accelerating rate as pressure rises. This is shown for $NaAlSi_3O_8$−H_2O in Fig. 3.5A. The inflection at ~1 GPa signals a change in the sign of the second derivative of H_2O solubility with pressure. Between 1.6 and 1.7 GPa, the first derivative of solubility with respect to pressure is infinity. At this point, H_2O and $NaAlSi_3O_8$ liquid become fully miscible, yielding a single phase typically termed a "supercritical fluid" (the term is used here exclusively in the context of complete mixing in multicomponent systems). Complete mixing occurs in simple systems as well as

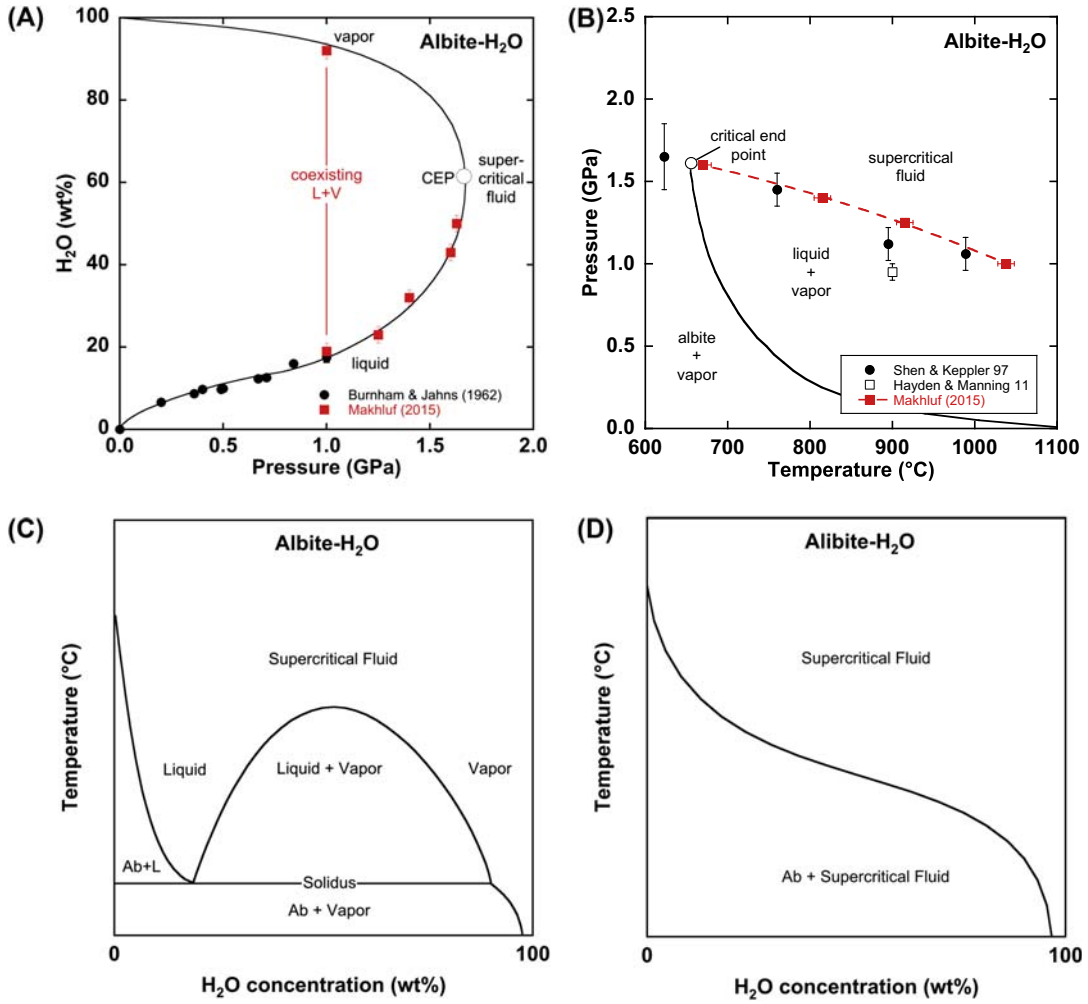

FIGURE 3.5

Phase relations in the system $NaAlSi_3O_8$–H_2O. (A) Polythermal variation in liquid–vapor solubility with pressure along the H_2O-saturated solidus. *Black circles*, Burnham and Jahns (1962); *red circles* (dark gray in print version), Makluf (2015, Ph.D. dissertation). (B) Pressure–temperature projection of the H_2O-saturated melting curve. The curve is terminated at the second critical end point where it intersects the liquid–vapor critical mixing curve. Data constraining the critical curve are from Shen and Keppler (1997, *black circles*), Hayden and Manning (2011, *black square*), and Makhluf (2015, Ph.D. dissertation, *red squares*). (C) Schematic T–X phase relations at subcritical pressure. (D) Schematic T–X phase relations at supercritical pressure.

natural silicate−H_2O systems at terrestrial conditions, though the pressure and temperature range at which this takes place varies strongly with composition. Previous reviews highlight the significance of supercritical fluids in a range of high-pressure environments (Manning, 2004; Hack et al., 2007a,b; Zheng et al., 2011; Hermann et al., 2013; Ni et al., 2017).

Fig. 3.5A shows that, at low, subcritical pressures, a saturated hydrous liquid coexists with a low-density, H_2O-rich vapor phase. As pressure increases the solubility of the hydrous melt in the vapor increases as H_2O solubility rises in the melt (Makhluf, 2015). The two solubility curves join at the second critical end point (CEP) on the hydrous melting curve. The CEP is defined by the intersection of the hydrous melting curve with the pressure−temperature trace of the critical mixing curve marking the crest of L = V solvus (Fig. 3.5B). Fig. 3.5C and D show schematic isobaric T-X diagrams for the system albite−H_2O at P < CEP and P > CEP, respectively. At P < CEP and subsolidus conditions, rising temperature results in increasing solubility of albite (Ab) in H_2O. Ab + H_2O melts to hydrous liquid at the solidus temperature T_s. Depending on bulk H_2O content, increasing temperature above T_s will yield Ab + hydrous liquid, hydrous liquid ± vapor, or solute-bearing vapor. Increasing temperature to T > CEP results in complete mixing between liquid and vapor. The range of composition of the supercritical fluid increases with rising temperature until, at the dry solidus, it spans the full Ab−H_2O binary. In contrast, at P > CEP, there is no discrete melting temperature. Instead, as temperature rises, solubility of Ab in H_2O increases dramatically over a finite temperature interval. Below this interval, Ab coexists with a phase with properties of the H_2O-rich vapor, whereas above, Ab coexists with a phase with properties of a hydrous liquid. Within the interval the fluid phase has properties intermediate between liquid and vapor. It is important to note that the term "supercritical fluid" applies to a fluid of any composition at pressure and temperature greater than the critical curve (Fig. 3.5B). (Some authors restrict use of the term to a fluid with arbitrary, intermediate composition; this is discouraged.)

Early experimental investigations hypothesizing critical mixing in silicate−H_2O systems required interpretations of quench textures whose ambiguities led to skepticism. For example, evidence for a second critical end point on the wet melting curve of quartz (Kennedy et al., 1962) was questioned by Stewart (1967) and Mysen (1998). However, independent solubility relations confirm critical mixing in the system at the conditions that Kennedy et al. (1962) proposed (Nakamura, 1974; Newton and Manning, 2008; Hunt and Manning, 2012). A wide range of techniques have now been applied to investigate critical mixing ranging from simple to complex systems (Boettcher and Wyllie, 1969; Paillat et al., 1992; Shen and Keppler, 1997; Bureau and Keppler, 1999; Stalder et al., 2000, 2001; Mibe et al., 2004, 2007, 2011; Kessel et al., 2005a,b; Hermann and Spandler, 2008; Hayden and Manning, 2011). The effusion of methodologies has led to controversy as to the pressure−temperature conditions of critical mixing in some key systems (Ni et al., 2017). For example, H_2O solubility in basaltic liquids is ~21 wt% at 1 GPa, suggesting a change with pressure similar to Fig. 3.5A (Mitchell et al., 2017). However, there is substantial disagreement on the location of the second critical end point on the hydrous basalt melting curve: it has been proposed to lie at 5.5 ± 0.5 GPa and 1050 ± 50°C by Kessel et al. (2005b), but at 3.4 GPa and 770°C by Mibe et al. (2011). The discrepancy arises from large uncertainty in the pressure−temperature trace of the critical curve. The nominally conflicting results might be explained by a large increase in the pressure−temperature slope of the curve in the vicinity of the end point (Ni et al., 2017), though such a change implies variations in entropy and/or

volume for which there is no independent evidence. More likely, detection of phase relations near end points is problematic for the methods used. The narrow two-phase loop separating liquid and vapor possessing very similar properties challenges detection limits in the X-ray radiography methods of Mibe et al. (2011). Similar issues may plague the conflicting results on the peridotite–H_2O system where discrepancies are even greater (Grove et al., 2006, 2012; Mibe et al., 2007; Till et al., 2012). In spite of disagreements about pressure–temperature locations, it should be noted that there is no disagreement as to the existence of CEP and supercritical fluids at some pressure–temperature for any of the systems considered here.

Why does complete mixing occur? As noted above, incorporation of H_2O into silicate is associated with depolymerization of the aluminosilicate network, pointing to a role for polymerization/depolymerization reactions in melt and coexisting fluid (Manning, 2004). Support for this inference can be found in studies of mineral solubility in H_2O, which show evidence for increasing polymerization of silicate and aluminosilicate species with rising solute concentrations at high pressure and temperature. Zotov and Keppler (2000, 2002) performed hydrothermal diamond-anvil experiments on the solubility of quartz in H_2O and detected an increasing concentration of aqueous silica dimers with rising pressure and temperature. This is consistent with excess silica solubility in the presence of quartz (Gerya et al., 2005; Newton and Manning, 2008) and at quartz undersaturation (Zhang and Frantz, 2000; Newton and Manning, 2002, 2003; Mysen et al., 2013). Manning et al. (2010) and Wohlers et al. (2011) inferred that a rapid increase in solute polymerization occurs near the solidus in hydrous albite-bearing systems. These observations imply that, just as depolymerization of hydrous silicate liquids is accompanied by rising H_2O concentration, so too is polymerization of dissolved silicate components accompanied by increasing solubility (i.e., decreasing H_2O concentration). Critical mixing in a given system simply occurs at pressure–temperature conditions where homogeneous polymerization/depolymerization reactions occur continuously across the binary, with no phase change.

Thermodynamic modeling of polymerization in the system SiO_2–H_2O (Hunt and Manning, 2012) shows that accounting solely for quartz solubility and mixing of H_2O, OH- and bridging O^{2-} (Eq. 3.1) correctly predicts the experimentally derived CEP and melting curve (Kennedy et al., 1962; Newton and Manning, 2008) and ab initio molecular dynamics calculations point to substantial polymerization at intermediate compositions (Spiekermann et al., 2016). This strongly supports the hypothesis that silicate–H_2O mixing properties are controlled by polymerization chemistry. Further support comes from the degree of silicate polymerization in hydrous Na–Al silicate systems (Mysen, 2014). Fig. 3.6 shows experimental results from isochoric hydrothermal diamond cell experiments in which pressure increases with temperature. This peralkaline system ($Na_6AlSi_9O_{22.5}$–H_2O) exhibits critical mixing with H_2O at ~600°C and 0.9 GPa. In the subcritical region, rising temperature (and pressure) causes NBO/T to decrease in the hydrous melt, indicating depolymerization. The NBO/T of solutes in the coexisting H_2O-rich phase is relatively unchanged, suggesting a steep solvus limb. A single phase with intermediate NBO/T is observed at ~610°C. The trend of NBO/T in the one-phase region indicates continued depolymerization of the supercritical fluid to higher pressure and temperature. Similar relations are seen in a less polymerized Na silicate bulk composition (Mysen, 2014).

The H_2O component in supercritical fluids is almost entirely molecular H_2O. As shown in Fig. 3.2, high bulk H_2O favors H_2O_{melt} over OH^-_{melt} at lower-crustal and upper-mantle pressures. For silicate melt–H_2O binaries, this implies that dissolved molecular H_2O is sufficient to disrupt the aluminosilicate network and drive depolymerization. First-principles simulations indicate that at transition-zone and

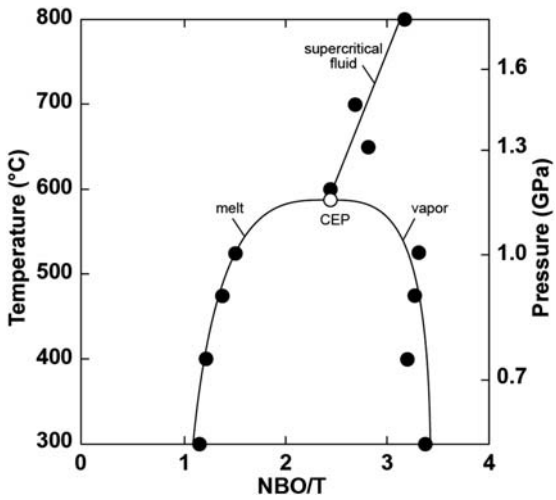

FIGURE 3.6

Variation in degree of polymerization (NBO/T) of $Na_6AlSi_9O_{22.5}$–H_2O with temperature and pressure. Results from Mysen (2007), determined by Raman spectroscopy in a hydrothermal diamond-anvil cell. Experiments are isochoric (pressure increases with temperature as shown on the right axis). The melt is more polymerized (lower NBO/T) than the vapor, but NBO/T increases with temperature. A single fluid is observed in the cell at $T > 600°C$; its NBO/T is intermediate between that of melt and vapor at lower temperature.

lower-mantle pressure, H_2O forms extended, polymerized structures linked to cation polyhedra, and H_2O–melt mixing tends toward ideality (Mookherjee et al., 2008; Bajgain et al., 2015). Thus, continuous polymerization/depolymerization reactions among melt polyhedral units and incorporation of molecular and extended forms of H_2O combine to cause supercritical mixing of all silicate melt–H_2O systems at high pressures.

Importantly, the activity of H_2O in supercritical fluids is high even at modest H_2O concentration (Fig. 3.7), at least at conditions corresponding to the lower crust and upper mantle. Makhluf et al. (2017b) combined constraints on liquidus relations in hydrous $NaAlSi_3O_8$ melts in the presence of CO_2 or NaCl with H_2O–CO_2 and H_2O–NaCl activity to derive a-X relations for H_2O in $NaAlSi_3O_8$–H_2O melts and fluids at 1 GPa. H_2O activity rises rapidly along the polythermal trace of the liquidus. At temperatures below the critical temperature of 1090°C (Makhluf et al., 2016), the shallowing slopes of isotherms with rising temperature indicate decreasing nonideality of mixing. At $T_c = 1090°C$, H_2O activity is ≥ 0.8 at $X_{H_2O} \geq 0.38$ (4 wt% H_2O). Thus, for a wide range of H_2O concentrations, the activity of H_2O is surprisingly close to one.

This has profound implications for the role of supercritical fluids in the mantle. A supercritical fluid produced by dehydration "melting" at P > CEP may be low in total fraction, but will have intermediate H_2O concentration and will possess H_2O activity sufficiently high ($a_{H_2O} = 0.8$–0.9) to have the chemical effects of nearly pure water. Such a fluid can readily trigger fluid-saturated, high a_{H_2O} melting along its flow path. A simple example is slab sediment "melts" contributing to the generation of arc magmas (e.g., Hermann and Spandler, 2008; Plank et al., 2009; Mallik et al., 2016). The results of Cooper et al. (2012) reveal that this situation may be common. Fig. 3.8 shows that of the 10 global

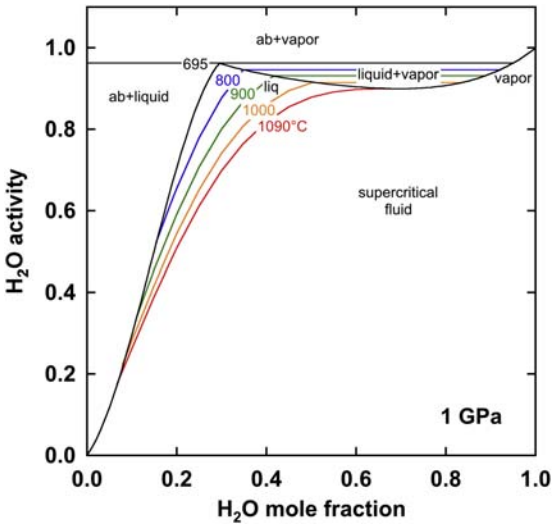

FIGURE 3.7

H_2O activity versus H_2O mole fraction in the system $NaAlSi_3O_8$–H_2O at 1.0 GPa. Mole fraction on a 1 oxygen basis. Liquidus (*black*) after Makhluf et al. (2017a,b). Isotherms in the liquid/supercritical fluid field (*colored lines*) and other phase boundaries (*black lines*) from Makhluf et al. (2016). The figure illustrates the high H_2O activity at modest H_2O concentration.

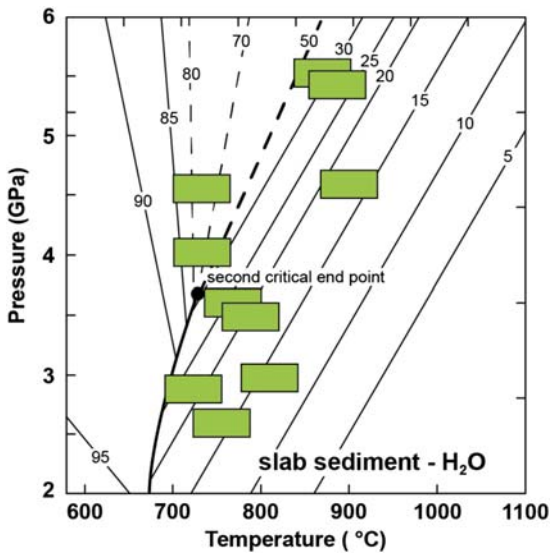

FIGURE 3.8

Melting and solubility relations for slab sediment–H_2O, from Hermann and Spandler (2008). Inferred solubility isopleths converge on the critical end point just below 4 GPa. *Green rectangles* reflect temperature calculated from H_2O/Ce thermometry and subarc depth to slab for 10 global subduction systems (Cooper et al., 2012).

subduction systems for which estimates could be made, five indicated pressure and temperature consistent with production of a supercritical fluid derived from sediment at the slab–mantle interface. There is also ample evidence of at least transient existence of hydrous supercritical fluids in other high-pressure contexts, including ultrahigh-pressure metamorphic rocks (Ferrando et al., 2005; Zhang et al., 2008; Zheng et al., 2011; Hermann et al., 2013; Zheng and Hermann, 2014; Huang and Xiao, 2015) and diamond genesis (Klein-BenDavid et al., 2007; Weiss et al., 2015).

4. PHYSICAL PROPERTIES OF HYDROUS SILICATE MELTS

4.1 VOLUME AND DENSITY

The density of silicate liquids in the lower crust and mantle exerts a fundamental control on mobility and seismic properties. At 1 bar, silicate melt densities are simple functions of the partial molar volumes of component oxides (Bottinga and Weill, 1970; Lange and Carmichael, 1987, 1989). The addition of H_2O increases the volume and decreases the density of a silicate melt. Experimental studies indicate that the partial molar volume of H_2O in hydrous silicate melts $\left(\overline{V}_{H_2O}\right)$ is lower than in free H_2O, and—crucially—appears to be independent of H_2O speciation or melt composition and structure (Orlova, 1964; Burnham and Davis, 1971; Ochs and Lange, 1997, 1999; Richet and Polian, 1998; Richet et al., 2000). $\overline{V}_{H_2O}$ possesses higher isothermal expansivity than other oxides, but expansivity is lower than that of free H_2O vapor.

Characterization of the changes in the density of hydrous silicate melts with pressure has long presented experimental challenges. Early dilatometry measurements on $NaAlSi_3O_8$–H_2O (Burnham and Davis, 1971, 1974) were exceptionally useful, but they were arduous, relatively restricted in pressure, and difficult to extend to other compositional systems. Studies of hydrous glasses quenched from high pressure and temperature demonstrated the compositional independence of $\overline{V}_{H_2O}$ (Ochs and Lange, 1997, 1999) but were limited with respect to the role of pressure. Sink-float experiments (Agee and Walker, 1988) permit bracketing of density at high pressure and temperature and have been deployed on a range of hydrous silicate melt compositions (Fig. 3.9A) (Matsukage et al., 2005; Sakamaki et al., 2006; Agee, 2008b; Jing and Karato, 2012). However, the nature of the experiment intrinsically limits the pressure, temperature, and composition space of a given study. Newly emerging X-ray absorption, diffraction, and imaging methods applied to hydrous silicate melts (e.g., Sakamaki et al., 2009; Malfait et al., 2014) hold great promise for expanding our understanding in the coming years. The experimental data have been incorporated into a variety of equations of state for $\overline{V}_{H_2O}$ and hydrous silicate melts to characterize changes in the volume with pressure (Agee, 2008a,b; Jing and Karato, 2009, 2012; Sakamaki et al., 2009; Malfait et al., 2014; Ueki and Iwamori, 2016).

Despite minor differences due to experimental methods and equation of state employed, there are several key conclusions that appear to be robust. All results indicate that, with rising pressure, the volume of a hydrous melt decreases to a greater extent than its anhydrous equivalent; that is, the H_2O component in melts is more compressible than other oxide components. At high pressure, the isobaric expansivity of H_2O in melts is lower than at low pressure, as is the case for pure H_2O. At all pressures, $\overline{V}_{H_2O}$ is less than the molar volume of pure H_2O, indicating that the volume change for the transfer of H_2O from the free vapor phase to a dissolved component in silicate melt, $H_2O_v = H_2O_{melt}$, is always negative. This helps explain why the solubility of H_2O in silicate melt rises with pressure (Figs. 3.1, 3.4, and 3.5).

On the atomic scale, the increasing density of anhydrous melt with pressure is partly a consequence of increasing coordination of constituent cations. Ab initio simulations indicate that the same is true for hydrous melts. However, the space available for molecular H_2O becomes very small, making it

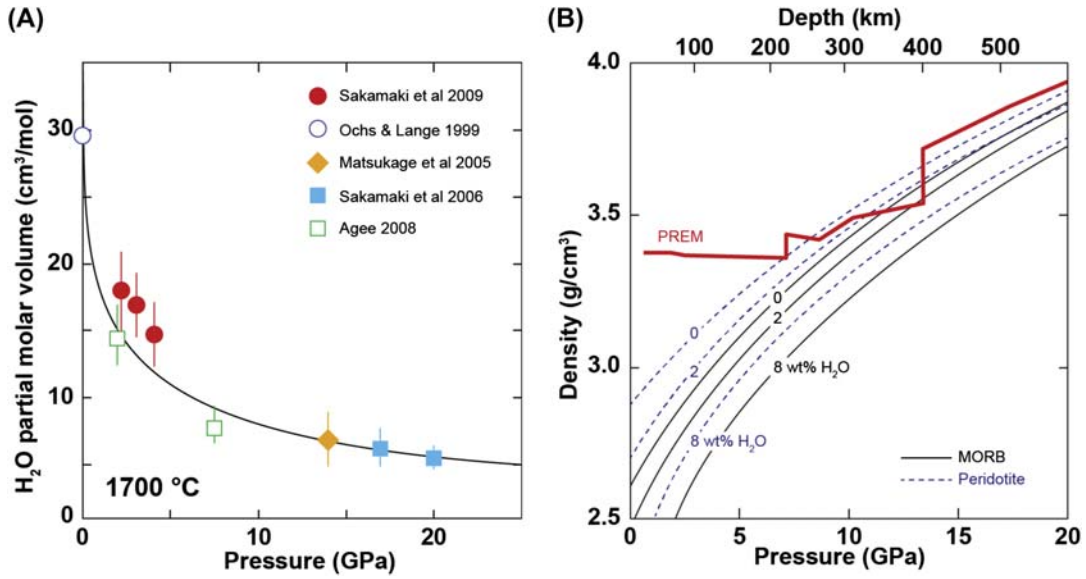

FIGURE 3.9

(A) Partial molar volume of H_2O in hydrous melts. Experimental data (Ochs and Lange, 1999; Matsukage et al., 2005; Sakamaki et al., 2006, 2009) corrected to 1700°C. $\overline{V}_{H_2O}$ is independent of melt composition. (B) Variation in density of basalt (*solid lines*) and peridotite (*dashed lines*) liquids with pressure and H_2O concentration, at 1600°C. Results are compared from the Preliminary Reference Earth Model (PREM, Dziewonski and Anderson, 1981), showing that basalt with $\lesssim$3 wt% H_2O and peridotite with $\lesssim$6 wt% H_2O are more dense than the mantle immediately above the 410-km discontinuity. Such liquids could therefore be trapped at this depth, supporting models of a transition-zone water filter (e.g., Bercovici and Karato, 2003).

relatively unstable compared to more compressed forms involving the extended linkages between melt units referred to in earlier sections (Mookherjee et al., 2008; Karki and Stixrude, 2010; Bajgain et al., 2015).

The seismic properties of hydrous melts are strongly influenced by H_2O content (Wu et al., 2014; Ueki and Iwamori, 2016). This has important consequences for the detection of hydrous melt in the mantle. Assuming that isothermal bulk modulus is equal to adiabatic bulk modulus, Ueki and Iwamori (2016) calculated the seismic velocities and V_p/V_s for partially molten mantle and lower crustal rocks at 1 GPa and 800−1000°C, relevant to the uppermost mantle wedge in a subduction zone. As with anhydrous melts, V_p drops with increasing melt fraction, but to a smaller degree as H_2O content increases. Similarly, V_p/V_s rises with melt fraction, but this grows less pronounced with increasing H_2O in the silicate melt. Notably, Ueki and Iwamori (2016) limit consideration to 6 wt% H_2O in the melt. Extending these results to deeper conditions will require accounting for the possibility of much higher H_2O concentrations.

Understanding the pressure−temperature dependence of density and seismic properties of hydrous silicate liquids is essential for testing hypotheses which invoke the ponding of hydrous silicate melt to explain geophysical anomalies in a variety of mantle environments. Key to such hypotheses is that

the melting temperature must be reduced by a fluxing agent such as H_2O, but density must remain sufficiently high to cause the melt to be neutrally buoyant at the depth of interest. Experimental and modeling investigations have shown that hydrous melts of plausible composition and H_2O content could be gravitationally stable at the top of the transition zone and elsewhere (Matsukage et al., 2005; Sakamaki et al., 2006; Agee, 2008b; Jing and Karato, 2009, 2012).

Fig. 3.9B uses results from Sakamaki et al. (2006) to illustrate that MORB and model transition-zone peridotite melts are gravitationally stable at ~410 km for H_2O contents up to ~3 and ~6 wt%, respectively, assuming constant temperature of 1600°C. However, the likely high H_2O content of transition-zone minerals yields peridotite liquids with as much as 10–15 wt% H_2O, which would be too buoyant to be trapped at 410 km in the model of Sakamaki et al. (2006). Jing and Karato (2012) evaluated several equations of state, a wider range of compositions, and accounted for temperature variations with depth. They concluded that hydrous peridotite with 10–15 wt% H_2O could be neutrally buoyant at 410 km depth; the addition of other volatiles, such as CO_2, increases trapping potential because their density is greater than that of H_2O. It is important to note that evaluations of gravitational stability based on one-dimensional profiles, as in Fig. 3.9B, should be made with caution in light of complex global variations in the interactions between slabs and the transition zone (Goes et al., 2017).

4.2 MELT CONNECTIVITY

Melt migration by porous flow at low differential stress and low buoyancy may be driven by surface tension (Watson, 1982), which, on the grain boundary scale, is controlled by the interfacial energy of contacting grains. Interfacial energy is a function of the dihedral angle defined by the intersection of grain edges and a melt-filled pore (Watson, 1982; von Bargen and Waff, 1986). When the dihedral angle is $\leq$60 degrees, the melt wets the grain boundaries, forming an interconnected network that permits melt migration. If the dihedral angle is higher, the melt remains trapped in pores in the absence of any dynamic transformation of the grain interfaces. Variations in dihedral angle reflect a strong dependence on chemical interaction between minerals and melt through dissolution and reprecipitation processes (Watson, 1982). Therefore, for hydrous melts, the dependence of mineral solubility and liquid composition on H_2O concentration should have an important influence on the melt's wetting properties and hence the matrix permeability.

Experimental investigations of wetting properties of rocks at high pressure have focused chiefly on (nominally) anhydrous melts and aqueous fluids. In solid monomineralic and polymineralic matrices of mantle minerals, nominally anhydrous basaltic liquids generally form triple junction pores with dihedral angles between 25 and 50 degrees consistent with a matrix favorable to melt migration (Waff and Bulau, 1979, 1982; Watson, 1982; Jurewicz and Jurewicz, 1986; Toramaru and Fujii, 1986; von Bargen and Waff, 1986). A possible exception is pyroxene-rich rocks (Fujii et al., 1986; Toramaru and Fujii, 1986), though likely only under very dry conditions and strong preferred orientations (von Bargen and Waff, 1986). At conditions relevant to deep crustal melting, a wide range of more siliceous, nominally anhydrous liquids also form dihedral angles <60 degrees with typical lower-crustal minerals (Laporte and Provost, 2000). Intriguingly, Maumus et al. (2004) concluded that nominally anhydrous SiO_2-rich melts hypothesized as transport agents in subduction zones form dihedral angles with olivine that are too high to admit substantial melt migration.

There have been comparatively few studies of the wetting properties of hydrous melts. Fujii et al. (1986) investigated the effect of H_2O saturation on melt dihedral angles in peridotite comprised of

olivine, plagioclase, and pyroxenes at 1.5 GPa and 1250°C. They found that whereas pyroxene-rich grain junctions may have dihedral angles >60 degrees under anhydrous conditions, H_2O saturation leads to lower angles and a connected melt phase. A key limitation of this work is that very large melt fractions are produced at H_2O saturation, which makes it difficult to compare the results with lower melt fractions used in nominally anhydrous systems. For example, Raterron et al. (1997) found that volumetrically minor early melt fractions at H_2O saturation may be very Si-rich and become trapped in grain boundaries, suggesting they form dihedral angles >60 degrees.

Insights can be gained from studies of the effect of H_2O on dihedral angles at subsolidus conditions. At low temperatures and crustal pressures, mean dihedral angles in olivine, pyroxene, quartz, and polymineralic aggregates equilibrated with $H_2O \pm CO_2$ are typically >60 degrees (e.g., Watson and Brenan, 1987; Watson and Lupulescu, 1993). However, Mibe et al. (1999) showed that dihedral angles formed by H_2O in forsterite decrease to <60 degrees with increasing temperature from 800 to 1200°C and 3−6 GPa. At these conditions, the solubility of forsterite in H_2O rises dramatically (Stalder et al., 2001).

Anticorrelation between solubility and dihedral angle is consistent with the hypothesis that dihedral angles <60 degrees are generated by dissolution−reprecipitation reactions with the fluid (Watson, 1982). If true, rising solubility should promote this behavior. Thus, H_2O may play a key role in enhancing wettability of grain boundaries by enhancing or shifting dissolution reactions. Addition of H_2O to the SiO_2-rich mantle metasomatic fluid studied by Maumus et al. (2004) so that it is a supercritical intermediate fluid would likely lead to much lower dihedral angles than they found for the dry system, and hence greater mobility.

4.3 VISCOSITY

Viscosity exerts a fundamental control on the mobility of silicate melts (e.g., Hess and Dingwell, 1996; Mysen and Richet, 2005; Giordano et al., 2008, and references therein). Most silicate melts are Newtonian liquids, or nearly so (e.g., Ni et al., 2015), and viscosity, η (Pa s), depends strongly on melt structure and temperature. Viscosity therefore varies over many orders of magnitude for the wide range in compositions and temperatures of terrestrial magmas.

On a molar basis, H_2O has a greater effect on viscosity than any other cation (e.g., Dingwell, 2015). Early work on the effect of water on melt viscosity confirmed a link between depolymerization and a decrease in melt viscosity (Friedman et al., 1963; Shaw, 1963; Burnham, 1975; Stolper, 1982b). Initial studies concluded that pressure had a negligible influence on the viscosities of hydrous melts (Schulze et al., 1996, 1999; Liebske et al., 2003). However, the studies covered a relatively narrow range of pressure, H_2O concentration, and viscosity, and it remained possible that there was a small pressure dependence, as in anhydrous silicate melts (Kushiro, 1976, 1978; Kushiro et al., 1976). Any pressure effect should be most evident in more polymerized liquids, such as rhyolite. Ardia et al. (2008) inferred a modest but nonnegligible dependence of viscosity on pressure in anhydrous and hydrous rhyolite liquids. Hui et al. (2009) used an independent approach to confirm a pressure effect of a magnitude similar to that of Ardia et al. (2008), though they proposed a nonlinear functional form for which the effect is greatest at low pressure and diminishes at higher pressure.

Fig. 3.10A and B show variations in the viscosity at high pressure (η_P) relative to that at ambient pressure ($\eta_{1\ bar}$) at 800 and 1350°C and different H_2O concentrations, using the linear model of

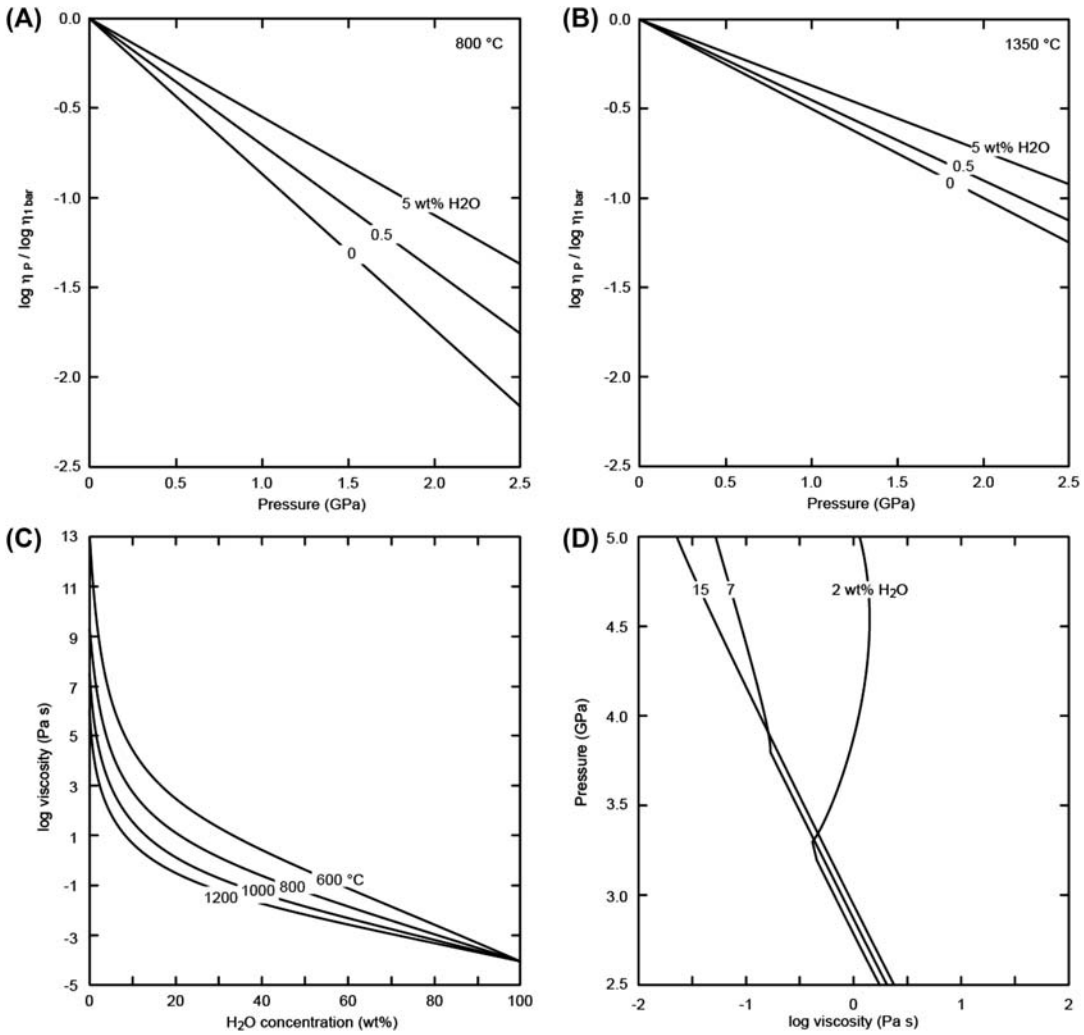

FIGURE 3.10

Viscosity of hydrous silicate melts at high pressure. (A) and (B) Relative change in viscosity of hydrous rhyolite melts with respect to 1 bar values at 800°C (A) and 1350°C (B), calculated from Ardia et al. (2008). (C) Change in viscosity with H_2O concentration for supercritical albite−H_2O fluids, at 600−1200°C (Audetat and Keppler, 2004). (D) Variation in viscosity of slab sediment melt along the solidus for 2, 7, and 15 wt% H_2O (Schmidt, 2015). Melt composition and temperature change with pressure. The 2 and 7 wt% H_2O compositions are undersaturated with H_2O at pressures above 3.2 and 3.7 GPa, respectively. Regardless of pressure (and temperature and composition), these melts possess low viscosity at all conditions shown.

Ardia et al. (2008). It can be seen that the viscosity of dry rhyolite liquid at 2.5 GPa is lower than at 1 bar by 2.2 and 1.2 log units at 800 and 1350°C, respectively. Addition of H_2O decreases the effect of pressure. For rhyolite with 5 wt% H_2O, the viscosity decreases from 1 bar to 2.5 GPa is only 1.3 and 0.9 log units at 800 and 1350°C, respectively.

The viscosity of H_2O-bearing rhyolite changes less with pressure than its anhydrous equivalent because H_2O addition at any pressure produces a dramatic depolymerization and viscosity reduction, dwarfing changes in pressure. Fig. 3.10C illustrates the effect of H_2O addition at high pressure for the system $NaAlSi_3O_8$–H_2O (Audetat and Keppler, 2004). The diagram reflects a compilation of results at 1.2–1.9 GPa assuming no pressure dependence and is relevant to near- and supercritical pressures. Viscosity of supercritical fluid along the $NaAlSi_3O_8$–H_2O join is a strongly nonlinear function of H_2O concentration. More than half of the decline (log units) with H_2O addition occurs in the first 10 wt% of H_2O (17 mol% on 1 oxygen basis). Fluids with >30 wt% H_2O have viscosities <1 Pa s, only modestly greater than the viscosity of pure H_2O ($\sim 10^{-4}$ Pa s). Models suggest that potassic fluids should have even lower viscosity (Hack and Thompson, 2011).

Schmidt (2015) calculated the viscosity of hydrous granitic liquid produced by the melting of subducted sediment. Fig. 3.10D shows viscosity variations with pressure at 2.5–5 GPa—pressures at which the temperature of melting increases with pressure. The viscosities of melts produced at the solidus lie in the relatively narrow range of $\sim 10^{-1.5}$–$10^{0.5}$ at the conditions portrayed. However, there are minor changes with pressure along the melting curve. The melts are saturated with H_2O at 15 wt% bulk H_2O, and viscosity decreases nearly linearly by $\sim 10^2$ from 5 to 2.5 GPa. Smaller declines are seen at 2 and 7 wt% H_2O. Departures from linearity arise from H_2O undersaturation at high pressure. The main controls on the viscosity variations are H_2O concentration, temperature, and to a lesser extent pressure, as melt composition changes little over this interval. A key observation is that, as shown in Fig. 3.10C, the viscosity of pure H_2O is only $\sim$2–4 log units lower than the hydrous silicate liquids. Such liquids must be highly mobile.

The viscosities of hydrous mafic and ultramafic liquids are likely less sensitive to pressure, at least over the pressure range shown in Fig. 3.10. However, the pronounced structural modifications induced by water at very high pressure (Bajgain et al., 2015) should be expressed in viscosity reduction as well.

4.4 ELECTRICAL CONDUCTIVITY AND DIFFUSIVITY

Electrical conductivity and diffusivity are closely linked properties because conductivity is controlled by the diffusivity of the most mobile ions in the liquid. Both parameters depend on pressure, temperature, bulk composition, and H_2O concentration. Focusing first on diffusivity, pressure and H_2O concentration have opposite effects for a given bulk composition and temperature, such that diffusivity declines with pressure but rises with H_2O content (Watson, 1981); major cations show different dependence on H_2O (see also Mysen and Richet, 2005, and references therein). First principles simulations yield similar results, except for SiO_2–H_2O, which shows an initial increase in Si, O, and H diffusivity with pressure (Karki and Stixrude, 2010).

Experimental characterization of the electrical conductivity of hydrous melts is challenging at high pressure, which limited the number of early investigations (Tyburczy and Waff, 1983). However, advances in impedance spectroscopy and sample confinement have enabled a surge in new studies (Gaillard, 2004; Pommier et al., 2008; Ni et al., 2011b). Gaillard (2004) proposed that Na is the primary charge carrier in hydrous natural siliceous melts. Conductivity increases with the addition of

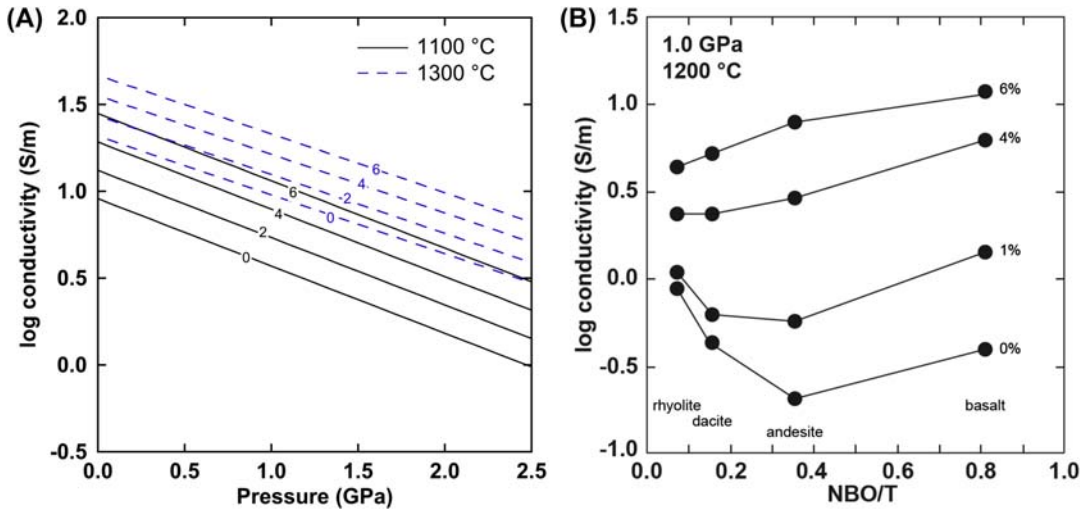

FIGURE 3.11

(A) Variation in electrical conductivity with pressure in hydrous $NaAlSi_3O_8$ melts. Calculated at 1100 (black) and 1300°C (*blue*; gray in print version) at 0–6 wt% H_2O, after Ni et al. (2011b). (B) Variation in electrical conductivity with melt composition and polymerization at 1200°C, from 0 to 6 wt% H_2O. Data at 1 GPa, except basalt at 2 GPa (Guo et al., 2017).

H_2O, but the effect is chiefly to increase the mobility of Na rather than the addition of H_2O dissociation products. That is, as with other properties, the primary influence of H_2O is through its modification of melt structure. Sodium was also found to be the primary charge carrier in hydrous albitic, dacitic, and basaltic liquids (Ni et al., 2011a,b; Laumonier et al., 2015). First principles simulations of simple Na-free compositional systems show that high proton mobility yields high conductivity (Mookherjee et al., 2008; Karki and Stixrude, 2010), suggesting that H^+ has a secondary but important role.

The roles of pressure, temperature, and H_2O on electrical conductivity can be illustrated using the model of Ni et al. (2011b) for $NaAlSi_3O_8$–H_2O (Fig. 3.11A). Electrical conductivity increases with rising temperature and H_2O concentration, but decreases with pressure. Limited experimental constraints suggest these trends continue to 10 GPa, at least for H_2O-poor liquids (Ni et al., 2011b). Models for more complex compositions yield similar trends, but appear to underestimate the effect of H_2O concentration (Pommier and Le-Trong, 2011).

Fig. 3.11B illustrates that electrical conductivity of hydrous melts is a comparatively weak function of melt structure, as reflected by bulk composition (Guo et al., 2017). At a given pressure and temperature and 4–6 wt% H_2O, conductivity increases with decreasing polymerization from rhyolite to basalt by about half an order of magnitude.

Calculation of electrical conductivities of hydrous silicate melts is essential for interpreting magnetotelluric survey data in, for example, subvolcanic regions and the mantle wedge above subduction zones (Pommier et al., 2008; Ni et al., 2011a,b; Laumonier et al., 2015; Guo et al., 2016, 2017). Of particular interest is that the presence of $\leq$1% hydrous silicate melt may afford sufficiently high bulk electrical conductivity to explain anomalously conductive regions corresponding to the

seismic low-velocity zone beneath midocean ridges (Evans et al., 2005; Baba et al., 2006), supporting hypotheses of deep hydrous melting beneath ridges (e.g., Hirschmann, 2010)—especially if CO_2 is also included (Sifré et al., 2014).

5. CONCLUDING REMARKS

Hydrous silicate melts are present in a wide range of deep terrestrial environments, and their properties exhibit important changes with pressure which influence their generation, composition, mobility, and detection. The pressure-dependent physical properties are expressions of H_2O concentration, and the manner in which H_2O interacts with and modifies the anhydrous structure of the liquid, regardless of the abundance and identity of hydrous species. For a given composition, H_2O content, and temperature, rising pressure decreases both the bulk melt volume and the molar volume of H_2O, as well as viscosity, conductivity, and diffusivity. Compressibility is enhanced. At high pressure, the solubility of H_2O becomes so great in silicate melts that fully miscible solutions likely form for all natural compositions. As with physical properties, this is a direct consequence of the role of H_2O in the polymerization chemistry of silicate systems. For many cases where hydrous silicate melts have been proposed to explain mantle geophysical anomalies—e.g., hydrous basalt at the top of the transition zone—the binary silicate−H_2O system is supercritical, permitting (but not requiring) very high H_2O concentrations at appropriate conditions. In any case, whether supercritical or subcritical, hydrous silicate melts are likely to be important geologic agents to at least as deep as the base of the transition zone.

ACKNOWLEDGMENTS

Supported by NSF grant EAR 1347987. The manuscript was improved by discussions with A. Makhluf, R. Newton, and C. Beghein.

REFERENCES

Agee, C.B., 2008a. Compressibility of water in magma and the prediction of density crossovers in mantle differentiation. Philos. Trans. R. Soc., A 366, 4239−4252.

Agee, C.B., 2008b. Static compression of hydrous silicate melt and the effect of water on planetary differentiation. Earth Planet. Sci. Lett. 265, 641−654.

Agee, C.B., Walker, D., 1988. Static compression and olivine flotation in ultrabasic silicate liquid. J. Geophys. Res. Solid Earth 93, 3437−3449.

Anderson, K.E., Grauvilardell, L.C., Hirschmann, M.M., Siepmann, J.I., 2008. Structure and speciation in hydrous silica melts. 2. Pressure effects. J. Phys. Chem. B 112, 13015−13021.

Annen, C., Blundy, J., Sparks, R., 2006. The genesis of intermediate and silicic magmas in deep crustal hot zones. J. Petrol. 47, 505−539.

Ardia, P., Giordano, D., Schmidt, M.W., 2008. A model for the viscosity of rhyolite as a function of H_2O-content and pressure: a calibration based on centrifuge piston cylinder experiments. Geochim. Cosmochim. Acta 72, 6103−6123.

Asimow, P.D., Dixon, J., Langmuir, C., 2004. A hydrous melting and fractionation model for mid-ocean ridge basalts: application to the mid-Atlantic ridge near the Azores. Geochem. Geophys. Geosyst. 5 (1).

Asimow, P.D., Langmuir, C., 2003. The importance of water to oceanic mantle melting regimes. Nature 421, 815−820.
Aubaud, C., Hauri, E.H., Hirschmann, M.M., 2004. Hydrogen partition coefficients between nominally anhydrous minerals and basaltic melts. Geophys. Res. Lett. 31, L20611.
Audetat, A., Keppler, H., 2004. Viscosity of fluids in subduction zones. Science 303, 513−516.
Baba, K., Chave, A.D., Evans, R.L., Hirth, G., Mackie, R.L., 2006. Mantle dynamics beneath the East Pacific rise at 17 S: insights from the mantle electromagnetic and tomography (MELT) experiment. J. Geophys. Res. Solid Earth 111.
Bajgain, S., Ghosh, D.B., Karki, B.B., 2015. Structure and density of basaltic melts at mantle conditions from first-principles simulations. Nat. Commun. 6.
Beghein, C., Yuan, K., Schmerr, N., Xing, Z., 2014. Changes in seismic anisotropy shed light on the nature of the Gutenberg discontinuity. Science 343, 1237−1240.
Bercovici, D., Karato, S.-i., 2003. Whole-mantle convection and the transition-zone water filter. Nature 425, 39−44.
Boettcher, A., Wyllie, P., 1969. The system CaO-SiO_2-CO_2-H_2O—III. Second critical end-point on the melting curve. Geochim. Cosmochim. Acta 33, 611−632.
Bolfan-Casanova, N., 2005. Water in the earth's mantle. Mineral. Mag. 69, 229−257.
Bottinga, Y., Weill, D.F., 1970. Densities of liquid silicate systems calculated from partial molar volumes of oxide components. Am. J. Sci. 269, 169−182.
Bureau, H., Keppler, H., 1999. Complete miscibility between silicate melts and hydrous fluids in the upper mantle: experimental evidence and geochemical implications. Earth Planet. Sci. Lett. 165, 187−196.
Burnham, C., 1979. The importance of volatile constituents. In: Yoder Jr., H.S. (Ed.), The Evolution of the Igneous Rocks: Fiftieth Anniversary Perspectives. Princeton University Press, Princeton, NJ, pp. 439−482.
Burnham, C.W., 1975. Water and magmas: a mixing model. Geochim. Cosmochim. Acta 39, 1077−1084.
Burnham, C.W., 1997. Magmas and hydrothermal fluids. In: Barnes, H.L. (Ed.), Geochemistry of Hydrothermal Ore Deposits. John Wiley and Sons, New York, pp. 63−123.
Burnham, C.W., Davis, N.F., 1971. The role of H_2O in silicate melts. I. P-V-T relations in the system $NaAlSi_3O_8$-H_2O to 10 kilobars and 1000 C. Am. J. Sci. 270, 54−79.
Burnham, C.W., Davis, N.F., 1974. The role of H_2O in silicate melts: II. Thermodynamic and phase relations in the system $NaAlSi_3O_8$-H_2O to 10 kilobars, 700 to 1100 C. Am. J. Sci. 274, 902−940.
Burnham, C.W., Jahns, R.H., 1962. A method for determining the solubility of water in silicate melts. Am. J. Sci. 260, 721−745.
Campbell, I., Taylor, S., 1983. No water, no granites-no oceans, no continents. Geophys. Res. Lett. 10, 1061−1064.
Cashman, K.V., Sparks, R.S.J., Blundy, J.D., 2017. Vertically extensive and unstable magmatic systems: a unified view of igneous processes. Science 355, eaag3055.
Cooper, L.B., Ruscitto, D.M., Plank, T., Wallace, P.J., Syracuse, E.M., Manning, C.E., 2012. Global variations in H_2O/Ce: 1. Slab surface temperatures beneath volcanic arcs. Geochem. Geophys. Geosyst. 13, Q03024.
Crépisson, C., Morard, G., Bureau, H., Prouteau, G., Morizet, Y., Petitgirard, S., Sanloup, C., 2014. Magmas trapped at the continental lithosphere−asthenosphere boundary. Earth Planet. Sci. Lett. 393, 105−112.
Dingwell, D.B., 2015. Properties of rocks and minerals−diffusion, viscosity, and flow of melts. In: Schubert, G. (Ed.), Treatise on Geophysics, second ed. Elsevier, Amsterdam.
Dingwell, D.B., 1986. Volatile Solubilities in Silicate Melts.
Dixon, J.E., Stolper, E.M., Holloway, J.R., 1995. An experimental study of water and carbon dioxide solubilities in mid-ocean ridge basaltic liquids. Part I: calibration and solubility models. J. Petrol. 36, 1607−1631.
Dziewonski, A.M., Anderson, D.L., 1981. Preliminary reference Earth model. Phys. Earth Planet. Inter. 25.4, 297−356.

Evans, R.L., Hirth, G., Baba, K., Forsyth, D., Chave, A., Mackie, R., 2005. Geophysical evidence from the MELT area for compositional controls on oceanic plates. Nature 437, 249–252.

Ferrando, S., Frezzotti, M., Dallai, L., Compagnoni, R., 2005. Multiphase solid inclusions in UHP rocks (Su-Lu, China): remnants of supercritical silicate-rich aqueous fluids released during continental subduction. Chem. Geol. 223, 68–81.

Friedman, I., Long, W., Smith, R.L., 1963. Viscosity and water content of rhyolite glass. J. Geophys. Res. 68, 6523–6535.

Fujii, N., Osamura, K., Takahashi, E., 1986. Effect of water saturation on the distribution of partial melt in the olivine-pyroxene-plagioclase system. J. Geophys. Res. 91, 9253–9259.

Gaetani, G.A., Grove, T.L., 1998. The influence of water on melting of mantle peridotite. Contrib. Mineral. Petrol. 131, 323–346.

Gaillard, F., 2004. Laboratory measurements of electrical conductivity of hydrous and dry silicic melts under pressure. Earth Planet. Sci. Lett. 218, 215–228.

Gerya, T.V., Maresch, W.V., Burchard, M., Zakhartchouk, V., Doltsinis, N.L., Fockenberg, T., 2005. Thermodynamic modeling of solubility and speciation of silica in H_2O-SiO_2 fluid up to 1300 C and 20 kbar based on the chain reaction formalism. Eur. J. Mineral. 17, 269–283.

Gerya, T.V., Yuen, D.A., 2003. Rayleigh–Taylor instabilities from hydration and melting propel "cold plumes" at subduction zones. Earth Planet. Sci. Lett. 212, 47–62.

Giordano, D., Russell, J.K., Dingwell, D.B., 2008. Viscosity of magmatic liquids: a model. Earth Planet. Sci. Lett. 271, 123–134.

Goes, S., Agrusta, R., van Hunen, J., Garel, F., 2017. Subduction-transition zone interaction: a review. Geosphere 13, 644–664.

Green, D., 1973. Experimental melting studies on a model upper mantle composition at high pressure under water-saturated and water-undersaturated conditions. Earth Planet. Sci. Lett. 19, 37–53.

Green, D.H., Hibberson, W.O., Kovács, I., Rosenthal, A., 2010. Water and its influence on the lithosphere-asthenosphere boundary. Nature 467, 448–451.

Grove, T.L., Chatterjee, N., Parman, S.W., Medard, E., 2006. The influence of H_2O on mantle wedge melting. Earth Planet. Sci. Lett. 249, 74–89.

Grove, T.L., Till, C.B., Krawczynski, M.J., 2012. The role of H_2O in subduction zone magmatism. Annu. Rev. Earth Planet. Sci. 40, 413–439.

Guo, X., Li, B., Ni, H., Mao, Z., 2017. Electrical conductivity of hydrous andesitic melts pertinent to subduction zones. J. Geophys. Res. Solid Earth 122, 1777–1788.

Guo, X., Zhang, L., Behrens, H., Ni, H., 2016. Probing the status of felsic magma reservoirs: constraints from the P–T–H_2O dependences of electrical conductivity of rhyolitic melt. Earth Planet. Sci. Lett. 433, 54–62.

Hack, A.C., Hermann, J., Mavrogenes, J.A., 2007a. Mineral solubility and hydrous melting relations in the deep earth: analysis of some binary A–H_2O system pressure-temperature-composition topologies. Am. J. Sci. 307, 833–855.

Hack, A.C., Thompson, A.B., Aerts, M., 2007b. Phase relations involving hydrous silicate melts, aqueous fluids, and minerals. Rev. Mineral. Geochem. 65, 129–185.

Hack, A.C., Thompson, A.B., 2011. Density and viscosity of hydrous magmas and related fluids and their role in subduction zone processes. J. Petrol. 52, 1333–1362.

Hayden, L.A., Manning, C.E., 2011. Rutile solubility in supercritical $NaAlSi_3O_8$–H_2O fluids. Chem. Geol. 284, 74–81.

Hermann, J., Spandler, C., 2008. Sediment melts at sub-arc depths: an experimental study. J. Petrol. 49, 717–740.

Hermann, J., Zheng, Y.-F., Rubatto, D., 2013. Deep fluids in subducted continental crust. Elements 9, 281–287.

Hess, K., Dingwell, D., 1996. Viscosities of hydrous leucogranitic melts: a non-Arrhenian model. Am. Mineral. 81, 1297–1300.

Hess, P.C., 1971. Polymer model of silicate melts. Geochim. Cosmochim. Acta 35, 289−306.
Hess, P.C., 1980. Polymerization model for silicate melts. In: Hargraves, R.B. (Ed.), Physics of Magmatic Processes. Princeton University Press, Princeton, New Jersey, pp. 3−49.
Hirschmann, M.M., 2006. Water, melting, and the deep earth H_2O cycle. Annu. Rev. Earth Planet. Sci. 34, 629−653.
Hirschmann, M.M., 2010. Partial melt in the oceanic low velocity zone. Phys. Earth Planet. Inter. 179, 60−71.
Hirschmann, M.M., Kohlstedt, D.L., 2012. Water in earth's mantle. Phys. Today 65, 40−45.
Hirth, G., Kohlsetdt, D.L., 1996. Water in the oceanic upper mantle: implications for rheology, melt extraction and the evolution of the lithosphere. Earth Planet. Sci. Lett. 144, 93−108.
Holland, T.J.B., Powell, R., 1998. An internally consistent thermodynamic data set for phases of petrological interest. J. Metamorphic Geol. 16, 309−343.
Holtz, F., Behrens, H., Dingwell, D.B., Johannes, W., 1995. H_2O solubility in haplogranitic melts: compositional, pressure, and temperature dependence. Am. Mineral 80, 94−108.
Huang, J., Xiao, Y., 2015. Element mobility in mafic and felsic ultrahigh-pressure metamorphic rocks from the Dabie UHP Orogen, China: insights into supercritical liquids in continental subduction zones. Int. Geol. Rev. 57, 1103−1129.
Hui, H., Zhang, Y., Xu, Z., Del Gaudio, P., Behrens, H., 2009. Pressure dependence of viscosity of rhyolitic melts. Geochim. Cosmochim. Acta 73, 3680−3693.
Hunt, J.D., Manning, C.E., 2012. A thermodynamic model for the system SiO_2-H_2O near the upper critical end point based on quartz solubility experiments at 500-1100 C and 5-20 kbar. Geochim. Cosmochim. Acta 86, 196−213.
Inoue, T., 1994. Effect of water on melting phase relations and melt composition in the system Mg_2SiO_4−$MgSiO_3$−H_2O up to 15 GPa. Phys. Earth Planet. Inter. 85, 237−263.
Jing, Z., Karato, S.-i., 2009. The density of volatile bearing melts in the earth's deep mantle: the role of chemical composition. Chem. Geol. 262, 100−107.
Jing, Z., Karato, S.-I., 2012. Effect of H_2O on the density of silicate melts at high pressures: static experiments and the application of a modified hard-sphere model of equation of state. Geochim. Cosmochim. Acta 85, 357−372.
Johannes, W., Holtz, F., 1996. Petrogenesis and Experimental Petrology of Granitic Rocks. Springer, Berlin.
Jurewicz, S.R., Jurewicz, A.J., 1986. Distribution of apparent angles on random sections with emphasis on dihedral angle measurements. J. Geophys. Res. Solid Earth 91, 9277−9282.
Karato, S.-i., 2011. Water distribution across the mantle transition zone and its implications for global material circulation. Earth Planet. Sci. Lett. 301, 413−423.
Karato, S.-i., Bercovici, D., Leahy, G., Richard, G., Jing, Z., 2006. The transition-zone water filter model for global material circulation: where do we stand? Earth's Deep Water Cycle 289−313.
Karki, B.B., Stixrude, L., 2010. First-principles study of enhancement of transport properties of silica melt by water. Phys. Rev. Lett. 104, 215901.
Katz, R.F., Spiegelman, M., Langmuir, C.H., 2003. A new parameterization of hydrous mantle melting. Geochem. Geophys. Geosyst. 4.
Kawamoto, T., Holloway, J.R., 1997. Melting temperature and partial melt chemistry of H_2O-saturated mantle peridotite to 11 gigapascals. Science 276, 240−243.
Kelley, K.A., Plank, T., Grove, T.L., Stolper, E.M., Newman, S., Hauri, E., 2006. Mantle melting as a function of water content beneath back-arc basins. J. Geophys. Res. Solid Earth 111.
Kelley, K.A., Plank, T., Newman, S., Stolper, E.M., Grove, T.L., Parman, S., Hauri, E.H., 2010. Mantle melting as a function of water content beneath the Mariana arc. J. Petrol. 51.
Kennedy, G.C., Wasserburg, G.J., Heard, H.C., Newton, R.C., 1962. The upper three-phase region in the system SiO_2-H_2O. Am. J. Sci. 260, 501−521.

Kessel, R., Fumagalli, P., Pettke, T., 2015. The behaviour of incompatible elements during hydrous melting of metasomatized peridotite at 4−6 GPa and 1000 °C−1200 °C. Lithos 236, 141−155.

Kessel, R., Schmidt, M.W., Ulmer, P., Pettke, T., 2005a. Trace element signature of subduction-zone fluids, melts and supercritical liquids at 120−180 km depth. Nature 437, 724−727.

Kessel, R., Ulmer, P., Pettke, T., Schmidt, M.W., Thompson, A.B., 2005b. The water-basalt system at 4 to 6 GPa: phase relations and second critical endpoint in a K-free eclogite at 700 to 1400 C. Earth Planet. Sci. Lett. 237, 873−892.

Klein-BenDavid, O., Izraeli, E.S., Hauri, E., Navon, O., 2007. Fluid inclusions in diamonds from the Diavik mine, Canada and the evolution of diamond-forming fluids. Geochim. Cosmochim. Acta 71, 723−744.

Kohlstedt, D., Keppler, H., Rubie, D., 1996. Solubility of water in the α, β and γ phases of $(Mg, Fe)_2SiO_4$. Contrib. Mineral. Petrol. 123, 345−357.

Kushiro, I., 1976. Changes in viscosity and structure of melt of $NaAlSi_2O_6$ composition at high pressures. J. Geophys. Res. 81, 6347−6350.

Kushiro, I., 1978. Viscosity and structural changes of albite ($NaAlSi_3O_8$) melt at high pressures. Earth Planet. Sci. Lett. 41, 87−90.

Kushiro, I., 1990. Partial melting of mantle wedge and evolution of island arc crust. J. Geophys. Res. Solid Earth 95, 15929−15939.

Kushiro, I., Syono, Y., Akimoto, S.-I., 1968a. Meltinig of a peridotite nodule at high pressures and high water pressures. J. Geophys. Res. 73, 6023−6029.

Kushiro, I., Yoder Jr., H.S., Nishikawa, M., 1968b. Effect of water on the melting of enstatite. Geol. Soc. Am. Bull. 79, 1685−1692.

Kushiro, I., Yoder Jr., H.S., Mysen, B.O., 1976. Viscosities of basalt and andesite melts at high pressures. J. Geophys. Res. 81, 6351−6356.

Lange, R.A., Carmichael, I.S.E., 1987. Densities of Na_2O-K_2O-CaO-MgO-FeO-Fe_2O_3-Al_2O_3-TiO_2-SiO_2 liquids: new measurements and derived partial molar properties. Geochim. Cosmochim. Acta 51, 2931−2946.

Lange, R.A., Carmichael, I.S.E., 1989. Ferric-ferrous equilibria in Na_2O-FeO-Fe_2O_3-SiO_2 melts: effects of analytical techniques on derived partial molar volumes. Geochim. Cosmochim. Acta 53, 2195−2204.

Laporte, D., Provost, A., 2000. The grain-scale distribution of silicate, carbonate and metallosulfide partial melts: a review of theory and experiments. Phys. Chem. Partial. Molten Rocks 93−140. Springer.

Laumonier, M., Gaillard, F., Sifre, D., 2015. The effect of pressure and water concentration on the electrical conductivity of dacitic melts: implication for magnetotelluric imaging in subduction areas. Chem. Geol. 418, 66−76.

Lee, S.K., Cody, G.D., Fei, Y., Mysen, B.O., 2004. Nature of polymerization and properties of silicate melts and glasses at high pressure. Geochim. Cosmochim. Acta 68, 4189−4200.

Liebske, C., Behrens, H., Holtz, F., Lange, R.A., 2003. The influence of pressure and composition on the viscosity of andesitic melts. Geochim. Cosmochim. Acta 67, 473−485.

Liu, Z., Park, J., Karato, S.-I., 2016. Seismological detection of low velocity anomalies surrounding the mantle transition zone in Japan subduction zone. Geophys. Res. Lett. 43.

Makhluf, A.R., 2015. Experimental Investigations at High Temperatures and Pressures on Melting and Mineral Solubility in Systems of Feldspars with Water, with Special Reference to the Origin of Granite. Ph.D. University of California, Los Angeles.

Makhluf, A.R., Newton, R.C., Manning, C.E., 2016. Hydrous albite magmas at lower crustal pressure: new results on liquidus H_2O content, solubility, and H_2O activity in the system $NaAlSi_3O_8$−H_2O−NaCl at 1.0 GPa. Contrib. Mineral. Petrol. 171, 75.

Makhluf, A.R., Newton, R.C., Manning, C.E., 2017a. Experimental determination of liquidus H_2O contents of haplogranite at deep-crustal conditions. Contrib. Mineral. Petrol. 172, 77.

Makhluf, A.R., Newton, R.C., Manning, C.E., 2017b. H_2O activity in albite melts at deep crustal P-T conditions derived from melting experiments in the systems $NaAlSi_3O_8$-H_2O-CO_2 and $NaAlSi_3O_8$-H_2O-NaCl. Petrology 25, 452−460.

Malfait, W.J., Seifert, R., Petitgirard, S., Mezouar, M., Sanchez-Valle, C., 2014. The density of andesitic melts and the compressibility of dissolved water in silicate melts at crustal and upper mantle conditions. Earth Planet. Sci. Lett. 393, 31−38.

Mallik, A., Dasgupta, R., Tsuno, K., Nelson, J., 2016. Effects of water, depth and temperature on partial melting of mantle-wedge fluxed by hydrous sediment-melt in subduction zones. Geochim. Cosmochim. Acta 195, 226−243.

Mann, U., Schmidt, M.W., 2015. Melting of pelitic sediments at subarc depths: 1. Flux vs. fluid-absent melting and a parameterization of melt productivity. Chem. Geol. 404, 150−167.

Manning, C.E., 2004. The chemistry of subduction-zone fluids. Earth Planet. Sci. Lett. 223, 1−16.

Manning, C.E., Antignano, A., Lin, H.A., 2010. Premelting polymerization of crustal and mantle fluids, as indicated by the solubility of albite+paragonite+quartz in H_2O at 1 GPa and 350-620 C. Earth Planet. Sci. Lett. 292, 325−336.

Matsukage, K.N., Jing, Z., Karato, S.-i., 2005. Density of hydrous silicate melt at the conditions of earth's deep upper mantle. Nature 438, 488−491.

Maumus, J., Laporte, D., Schiano, P., 2004. Dihedral angle measurements and infiltration property of SiO_2-rich melts in mantle peridotite assemblages. Contrib. Mineral. Petrol. 148, 1−12.

Mibe, K., Fujii, T., Yasuda, A., 1999. Control of the location of the volcanic front in island arcs by aqueous fluid connectivity in the mantle wedge. Nature 401, 259−262.

Mibe, K., Kanzaki, M., Kawamoto, T., Matsukage, K.N., Fei, Y.W., Ono, S., 2004. Determination of the second critical end point in silicate-H_2O systems using high-pressure and high-temperature X-ray radiography. Geochim. Cosmochim. Acta 68, 5189−5195.

Mibe, K., Kanzaki, M., Kawamoto, T., Matsukage, K.N., Fei, Y.W., Ono, S., 2007. Second critical endpoint in the peridotite-H_2O system. J. Geophys. Res. 112.

Mibe, K., Kawamoto, T., Matsukage, K.N., Fei, Y.W., Ono, S., 2011. Slab melting versus slab dehydration in subduction-zone magmatism. Proc. Natl. Acad. Sci. U.S.A. 108, 8177−8182.

Millhollen, G., Irving, A., Wyllie, P., 1974. Melting interval of peridotite with 5.7 percent water to 30 kilobars. J. Geol. 82, 575−587.

Mitchell, A.J., Gaetani, G.A., O'Leary, J.A., Hauri, E.H., 2017. H_2O solubility in basalt at upper mantle conditions. Contrib. Mineral. Petrol. 172, 85.

Mookherjee, M., Stixrude, L., Karki, B., 2008. Hydrous silicate melt at high pressure. Nature 452, 983−986.

Moore, G., Vennemann, T., Carmichael, I., 1998. An empirical model for the solubility of H_2O in magmas to 3 kilobars. Am. Mineral. 83, 36−42.

Müntener, O., Kelemen, P.B., Grove, T.L., 2001. The role of H_2O during crystallization of primitive arc magmas under uppermost mantle conditions and genesis of igneous pyroxenites: an experimental study. Contrib. Mineral. Petrol. 141, 643−658.

Myhill, R., Frost, D., Novella, D., 2017. Hydrous melting and partitioning in and above the mantle transition zone: insights from water-rich MgO-SiO_2-H_2O experiments. Geochim. Cosmochim. Acta 200, 408−421.

Mysen, B.O., 2014. Water-melt interaction in hydrous magmatic systems at high temperature and pressure. Prog. Earth Planet. Sci. 1, 4.

Mysen, B.O., Mibe, K., Chou, I.M., Bassett, W., 2013. Structure and equilibria among silicate species in aqueous fluids in the upper mantle: experimental SiO_2−H_2O and MgO−SiO_2−H_2O data recorded in situ to 900 C and 5.4 GPa. J. Geophys. Res. 118, 6076−6085.

Mysen, B.O., 1988. Structure and Properties of Silicate Melts. Elsevier, Amsterdam.

Mysen, B.O., 1998. Interaction between aqueous fluid and silicate melt in the pressure and temperatures regime of the earth's crust and upper mantle. Neues Jahrb. Mineral. Abh. 172, 227–244.

Mysen, B.O., 2007. The solution behavior of H_2O in peralkaline aluminosilicate melts at high pressure with implications for properties of hydrous melts. Geochim. Cosmochim. Acta 71, 1820–1834.

Mysen, B.O., Boettcher, A.L., 1975. Melting of a hydrous mantle: I. Phase relations of natural peridotite at high pressures and temperatures with controlled activities of water, carbon dioxide, and hydrogen. J. Petrol. 16, 520–548.

Mysen, B.O., Richet, P., 2005. Silicate Glasses and Melts: Properties and Structure. Elsevier, Amsterdam.

Nakamura, Y., 1974. The System SiO_2-H_2O-H_2 at 15 kbar, 73. Carnegie Institution of Washington Yearbook, pp. 259–263.

Newton, R.C., Manning, C.E., 2002. Solubility of silica in equilibrium with enstatite, forsterite, and H_2O at deep crust/upper mantle pressures and temperatures and an activity-concentration model for polymerization of aqueous silica. Geochim. Cosmochim. Acta 66, 4165–4176.

Newton, R.C., Manning, C.E., 2003. Activity coefficient and polymerization of aqueous silica at 800 C, 12 kbar, from solubility measurements on SiO_2-buffering mineral assemblages. Contrib. Mineral. Petrol. 146, 135–143.

Newton, R.C., Manning, C.E., 2008. Thermodynamics of SiO_2-H_2O fluid near the upper critical end point from quartz solubility measurements at 10 kbar. Earth Planet. Sci. Lett. 274, 241–249.

Ni, H., Hui, H., Steinle-Neumann, G., 2015. Transport properties of silicate melts. Rev. Geophys. 53, 715–744.

Ni, H., Keppler, H., Behrens, H., 2011a. Electrical conductivity of hydrous basaltic melts: implications for partial melting in the upper mantle. Contrib. Mineral. Petrol. 162, 637–650.

Ni, H., Keppler, H., Manthilake, M., Katsura, T., 2011b. Electrical conductivity of dry and hydrous $NaAlSi_3O_8$ glasses and liquids at high pressures. Contrib. Mineral. Petrol. 162, 501–513.

Ni, H., Zhang, L., Xiong, X., Mao, Z., Wang, J., 2017. Supercritical fluids at subduction zones: evidence, formation condition, and physicochemical properties. Earth Sci. Rev. 167.

Novella, D., Dolejš, D., Myhill, R., Pamato, M.G., Manthilake, G., Frost, D.J., 2017. Melting phase relations in the systems Mg_2SiO_4-H_2O and $MgSiO_3$-H_2O and the formation of hydrous melts in the upper mantle. Geochim. Cosmochim. Acta 204.

Ochs, F.A., Lange, R.A., 1997. The partial molar volume, thermal expansivity, and compressibility of H_2O in $NaAlSi_3O_8$ liquid: new measurements and an internally consistent model. Contrib. Mineral. Petrol. 129, 155–165.

Ochs, F.A., Lange, R.A., 1999. The density of hydrous magmatic liquids. Science 283, 1314–1317.

Orlova, G., 1964. Solubility of water in albite melts-under pressure. Int. Geol. Rev. 6, 254–258.

Paillat, O., Elphick, S.C., Brown, W.L., 1992. The solubility of water in $NaAlSi_3O_8$ melts: a re-examination of Ab-H_2O phase relationships and critical behaviour at high pressures. Contrib. Mineral. Petrol. 112, 490–500.

Palot, M., Jacobsen, S., Townsend, J., Nestola, F., Marquardt, K., Miyajima, N., Harris, J., Stachel, T., McCammon, C., Pearson, D., 2016. Evidence for H_2O-bearing fluids in the lower mantle from diamond inclusion. Lithos 265, 237–243.

Pearson, D., Brenker, F., Nestola, F., McNeill, J., Nasdala, L., Hutchison, M., Matveev, S., Mather, K., Silversmit, G., Schmitz, S., 2014. Hydrous mantle transition zone indicated by ringwoodite included within diamond. Nature 507, 221–224.

Perchuk, L.L., Kushiro, I., 1991. Thermodynamics of the liquidus in the system diopside—water: a review. Phys. Chem. Magmas 249–267. Springer, New York, NY.

Plank, T., Cooper, L.B., Manning, C.E., 2009. Emerging geothermometers for estimating slab surface temperatures. Nat. Geosci. 2, 611–615.

Plank, T., Kelley, K.A., Zimmer, M.M., Hauri, E.H., Wallace, P.J., 2013. Why do mafic arc magmas contain ~4 wt % water on average? Earth Planet. Sci. Lett. 364, 168–179.

Pöhlmann, M., Benoit, M., Kob, W., 2004. First-principles molecular-dynamics simulations of a hydrous silica melt: structural properties and hydrogen diffusion mechanism. Phys. Rev. B 70, 184209.

Poli, S., Schmidt, M.W., 1995. H_2O transport and release in subduction zones: experimental constraints on basaltic and andesitic systems. J. Geophys. Res. 100, 22299–22314.

Poli, S., Schmidt, M.W., 2002. Petrology of subducted slabs. Annu. Rev. Earth Planet. Sci. 30, 207–235.

Pommier, A., Gaillard, F., Pichavant, M., Scaillet, B., 2008. Laboratory measurements of electrical conductivities of hydrous and dry Mount Vesuvius melts under pressure. J. Geophys. Res. Solid Earth 113.

Pommier, A., Le-Trong, E., 2011. "SIGMELTS": a web portal for electrical conductivity calculations in geosciences. Comput. Geosci. 37, 1450–1459.

Raterron, P., Bussod, G.Y., Doukhan, N., Doukhan, J.-C., 1997. Early partial melting in the upper mantle: an AEM study of a lherzolite experimentally annealed at hypersolidus conditions. Tectonophysics 279, 79–91.

Revenaugh, J., Sipkin, S., 1994. Seismic evidence for melt atop the 410-km mantle discontinuity. Nature 369, 474–476.

Richet, P., Polian, A., 1998. Water as a dense icelike component in silicate glasses. Science 281, 396–398.

Richet, P., Whittington, A., Holtz, F., Behrens, H., Ohlhorst, S., Wilke, M., 2000. Water and the density of silicate glasses. Contrib. Mineral. Petrol. 138, 337–347.

Sakamaki, T., Ohtani, E., Urakawa, S., Suzuki, A., Katayama, Y., 2009. Measurement of hydrous peridotite magma density at high pressure using the X-ray absorption method. Earth Planet. Sci. Lett. 287, 293–297.

Sakamaki, T., Suzuki, A., Ohtani, E., 2006. Stability of hydrous melt at the base of the earth's upper mantle. Nature 439, 192–194.

Sakamaki, T., Suzuki, A., Ohtani, E., Terasaki, H., Urakawa, S., Katayama, Y., Funakoshi, K.-i., Wang, Y., Hernlund, J.W., Ballmer, M.D., 2013. Ponded melt at the boundary between the lithosphere and asthenosphere. Nat. Geosci. 6, 1041–1044.

Schmandt, B., Jacobsen, S.D., Becker, T.W., Liu, Z., Dueker, K.G., 2014. Dehydration melting at the top of the lower mantle. Science 344, 1265–1268.

Schmerr, N., 2012. The Gutenberg discontinuity: melt at the lithosphere-asthenosphere boundary. Science 335, 1480–1483.

Schmidt, M.W., 2015. Melting of pelitic sediments at subarc depths: 2. Melt chemistry, viscosities and a parameterization of melt composition. Chem. Geol. 404, 168–182.

Schmidt, M.W., Poli, S., 1998. Experimentally based water budgets for dehydrating slabs and consequences for arc magma generation. Earth Planet. Sci. Lett. 163, 361–379.

Schmidt, M.W., Vielzeuf, D., Auzanneau, E., 2004. Melting and dissolution of subducting crust at high pressures: the key role of white mica. Earth Planet. Sci. Lett. 228, 65–84.

Schulze, F., Behrens, H., Holtz, F., Roux, J., Johannes, W., 1996. The influence of H_2O on the viscosity of a haplogranitic melt. Am. Mineral. 81, 1155–1165.

Schulze, F., Behrens, H., Hurkuck, W., 1999. Determination of the influence of pressure and dissolved water on the viscosity of highly viscous melts: application of a new parallel-plate viscometer. Am. Mineral. 84, 1512–1520.

Shaw, H.R., 1963. Obsidian-H_2O viscosities at 1000 and 2000 bars in the temperature range 700 to 900 C. J. Geophys. Res. 68, 6337–6343.

Shen, A., Keppler, H., 1995. Infrared spectroscopy of hydrous silicate melts to 1000 C and 10 kbar: direct observation of H_2O speciation in a diamond-anvil cell. Am. Mineral. 80, 1335–1338.

Shen, A., Keppler, H., 1997. Direct observation of complete miscibility in the albite-H_2O system. Nature 385, 710–712.

Sifré, D., Gardés, E., Massuyeau, M., Hashim, L., Hier-Majumder, S., Gaillard, F., 2014. Electrical conductivity during incipient melting in the oceanic low-velocity zone. Nature 509, 81–85.

Silver, L., Stolper, E., 1985. A thermodynamic model for hydrous silicate melts. J. Geol. 93, 161–178.

Silver, L., Stolper, E., 1989. Water in albitic glasses. J. Petrol. 30, 667–709.
Silver, L.A., Ihninger, P.D., Stolper, E., 1990. The influence of bulk composition on the speciation of water in silicate glasses. Contrib. Mineral. Petrol. 104, 142–162.
Sowerby, J.R., Keppler, H., 1999. Water speciation in rhyolitic melt determined by in-situ infrared spectroscopy. Am. Mineral. 84, 1843–1849.
Spiekermann, G., Wilke, M., Jahn, S., 2016. Structural and dynamical properties of supercritical H_2O–SiO_2 fluids studied by ab initio molecular dynamics. Chem. Geol. 426, 85–94.
Stalder, R., Ulmer, P., Thompson, A.B., Guenter, D., 2000. Experimental approach to constrain second critical end points in fluid/silicate systems: near-solidus fluids and melts in the system albite-H_2O. Am. Mineral. 85, 68–77.
Stalder, R., Ulmer, P., Thompson, A.B., Gunther, D., 2001. High pressure fluids in the system MgO-SiO_2-H_2O under upper mantle conditions. Contrib. Mineral. Petrol. 140, 607–618.
Stewart, D.B., 1967. Four-phase curve in the systems $CaAl_2Si_2O_8$-SiO_2-H_2O between 1 and 10 kilobars. Schweiz. Mineral. Petrogr. 47, 35–59.
Stolper, E., 1982a. The speciation of water in silicate melts. Geochim. Cosmochim. Acta 46, 2609–2620.
Stolper, E., 1982b. Water in silicate glasses: an infrared spectroscopic study. Contrib. Mineral. Petrol. 81, 1–17.
Stolper, E., Newman, S., 1994. The role of water in the petrogenesis of Mariana trough magmas. Earth Planet. Sci. Lett. 121, 293–325.
Tauzin, B., Debayle, E., Wittlinger, G., 2010. Seismic evidence for a global low-velocity layer within the earth's upper mantle. Nat. Geosci. 3, 718–721.
Tenner, T.J., Hirschmann, M.M., Humayun, M., 2012. The effect of H_2O on partial melting of garnet peridotite at 3.5 GPa. Geochem. Geophys. Geosys. 13, Q03016.
Till, C.B., Grove, T.L., Withers, A.C., 2012. The beginnings of hydrous mantle wedge melting. Contrib. Mineral. Petrol. 163, 669–688.
Toffelmier, D.A., Tyburczy, J.A., 2007. Electromagnetic detection of a 410-km-deep melt layer in the southwestern United States. Nature 447, 991–994.
Toop, G., Samis, C., 1962. Activities of ions in silicate melts. Trans. Metall. Soc. AIME 224, 878–887.
Toramaru, A., Fujii, N., 1986. Connectivity of melt phase in a partially molten peridotite. J. Geophys. Res. Solid Earth 91, 9239–9252.
Tyburczy, J.A., Waff, H.S., 1983. Electrical conductivity of molten basalt and andesite to 25 kilobars pressure: geophysical significance and implications for charge transport and melt structure. J. Geophys. Res. Solid Earth 88, 2413–2430.
Ueki, K., Iwamori, H., 2016. Density and seismic velocity of hydrous melts under crustal and upper mantle conditions. Geochem. Geophys. Geosyst. 17, 1799–1814.
Ulmer, P., 2001. Partial melting in the mantle wedge—the role of H_2O in the genesis of mantle-derived "arc-related" magmas. Phys. Earth Planet. Inter. 127, 215–232.
van Keken, P.E., Hacker, B.R., Syracuse, E.M., Abers, G.A., 2011. Subduction factory: 4. Depth-dependent flux of H_2O from subducting slabs worldwide. J. Geophys. Res. 116, B01401.
von Bargen, N., Waff, H.S., 1986. Permeabilities, interfacial areas and curvatures of partially molten systems: results of numerical computations of equilibrium microstructures. J. Geophys. Res. 91, 9261–9276.
Waff, H., Bulau, J., 1982. Experimental determination of near-equilibrium textures in partially molten silicates at high pressures. In: High-Pressure Research in Geophysics, Advances in Earth and Planetary Sciences, vol. 12, pp. 229–236.
Waff, H.S., Bulau, J.R., 1979. Equilibrium fluid distribution in partial melt under hydrostatic stress conditions. J. Geophys. Res. 84, 6109–6114.
Wang, X.-C., Wilde, S.A., Li, Q.-L., Yang, Y.-N., 2015. Continental flood basalts derived from the hydrous mantle transition zone. Nat. Commun. 6, 7700.

Watson, E.B., 1981. Diffusion in magmas at depth in the earth: the effects of pressure and dissolved H_2O. Earth Planet. Sci. Lett. 52, 291–301.

Watson, E.B., 1982. Melt infiltration and magma evolution. Geology 10, 236–240.

Watson, E.B., Brenan, J.M., 1987. Fluids in the lithosphere. 1. Experimentally-determined wetting characteristics of CO_2-H_2O fluids and their implications for fluid transport, host-rock physical properties, and fluid inclusion formation. Earth Planet. Sci. Lett. 85, 497–515.

Watson, E.B., Lupulescu, A., 1993. Aqueous fluid connectivity and chemical transport in clinopyroxene-rich rocks. Earth Planet. Sci. Lett. 117, 279–294.

Weiss, Y., McNeill, J., Pearson, D.G., Nowell, G.M., Ottley, C.J., 2015. Highly saline fluids from a subducting slab as the source for fluid-rich diamonds. Nature 524, 339–342.

Wohlers, A., Manning, C.E., Thompson, A.B., 2011. Experimental investigation of the solubility of albite and jadeite in H_2O, with paragonite plus quartz at 500 and 600 C, and 1-2.25 GPa. Geochim. Cosmochim. Acta 75, 2924–2939.

Wu, L., Yang, D.-B., Xie, H.-S., Li, F.-F., Hu, B., Yu, Y., Xu, W.-L., Gao, C.-X., 2014. Pressure-induced elastic and structural changes in hydrous basalt glasses: the effect of H_2O on the gravitational stability of basalt melts at the base of the upper mantle. Earth Planet. Sci. Lett. 406, 165–173.

Zhang, Y., 1999. H_2O in rhyolitic glasses and melts: measurement, speciation, solubility, and diffusion. Rev. Geophys. 37, 493–516.

Zhang, Y.G., Frantz, J.D., 2000. Enstatite-forsterite-water equilibria at elevated temperatures and pressures. Am. Mineral. 85, 918–925.

Zhang, Z.-M., Shen, K., Sun, W.-D., Liu, Y.-S., Liou, J., Shi, C., Wang, J.-L., 2008. Fluids in deeply subducted continental crust: petrology, mineral chemistry and fluid inclusion of UHP metamorphic veins from the Sulu orogen, eastern China. Geochim. Cosmochim. Acta 72, 3200–3228.

Zheng, Y.-F., Hermann, J., 2014. Geochemistry of continental subduction-zone fluids. Earth Planets Space 66, 1–16.

Zheng, Y.F., Xia, Q.X., Chen, R.X., Gao, X.Y., 2011. Partial melting, fluid supercriticality and element mobility in ultrahigh-pressure metamorphic rocks during continental collision. Earth Sci. Rev. 107, 342–374.

Zotov, N., Keppler, H., 2000. In-situ Raman spectra of dissolved silica species in aqueous fluids to 900°C and 14 kbar. Am. Mineral. 85, 600–604.

Zotov, N., Keppler, H., 2002. Silica speciation in aqueous fluids at high pressures and high temperatures. Chem. Geol. 184, 71–82.